Basin Research

IAS EAGE

Basin Research (2011) 23, 257–290, doi: 10.1111/j.1365-2117.2010.00490.x

Lithospheric folding and sedimentary basin evolution: a review and analysis of formation mechanisms

Sierd Cloetingh* and Evgenii Burov†

*Netherlands Research Centre for Integrated Solid Earth Sciences, Faculty of Earth and Life Sciences, VU University, Amsterdam, The Netherlands

†Laboratoire de Tectonique, Université Pierre et Marie Curie, Paris Cedex 05, France

ABSTRACT

Lithospheric folding is an important mode of basin formation in compressional intraplate settings. Basins formed by lithospheric folding are characterized by distinct features in subsidence history. A comparison with extensional basins, foreland basins, intracratonic basins and pull-apart basins provides criteria for the discrimination between these modes of basin formation. These findings are important in deciphering the feedbacks between tectonics and surface processes. In addition, inferences on accommodation space and thermal regime have important consequences for hydrocarbon maturity. Lithospheric folding is coupled to compressional reactivation of basins and faults, and therefore, strongly affects reservoir characteristics of sedimentary basins.

INTRODUCTION

Over the last few years, much progress has been made in understanding the mechanisms of the formation of sedimentary basins (Cloetingh & Ziegler, 2007; Roure *et al.*, 2010). Quantitative models for several basin types have significantly advanced the understanding of extensional basins (EB) (McKenzie, 1978; Van Wees *et al.*, 2009) and foreland basins (FB) (Beaumont, 1981; Naylor & Sinclair, 2008). The mechanisms of basin formation as a result of lithospheric folding have received considerably less attention (Cloetingh & Ziegler, 2007) except for some clear-cut cases, in particular, in central Asia (Burov & Molnar, 1998; Thomas *et al.*, 1999a, b). Many data exist on the geometry of sedimentary basins affected by large-scale compressional intraplate deformation (Cobbold *et al.*, 1993; Lefort & Agarwal, 1996, 2000, 2002; Burov & Molnar, 1998). These observations and results of analytical, numerical (Martinod & Davy, 1992; Burov *et al.*, 1993; Gerbault *et al.*, 1998; Cloetingh *et al.*, 1999) and analogue modelling (Martinod & Davy, 1994; Sokoutis *et al.*, 2005) demonstrate that the thermo-mechanical age of the lithosphere exerts a prime control on the wavelength of lithospheric folds. These studies focused on the role of tectonic stress in lithospheric folding (Stephenson *et al.*, 1990; Stephenson & Cloetingh, 1991; Burov & Molnar, 1998). However, surface processes also play a significant role in the mechanics of lithospheric folding. Erosion enhances the development of folding and has a pronounced effect on its wavelengths (Cloetingh *et al.*, 1999; Burov & Toussaint, 2007), specifically in the short-wavelength domain. In addition, both sedimentation and erosion are likely to significantly prolong the lifetime of folding. Sedimentation decreases the effect of gravity by filling the downward flexed basins and thus reducing the isostatic restoring force, whereas erosion of the upward flexed basement unloads the lithosphere on the basins' uplifted flanks. Lithospheric folding has significant effects for the geometry of sedimentary sequences deposited on folded lithosphere. However, the effect has been little studied for several reasons (Cobbold *et al.*, 1993). The hanging walls of emerging low-angle thrust faults tend to collapse rapidly, blurring the structural relationships at basin edges. Further, ongoing sedimentation may onlap and bury the hanging walls, whereas scarp erosion may destroy them. Seismic images of basin edges may not be well resolved where footwall conglomerates contain few reflecting horizons or when low-angle thrusts reflect and refract seismic waves, thus hampering the imaging of deeper parts of the basin. Downwarping of folded basins renders surface geological mapping difficult. At the same time, high plateaux are not at first sight linked with basins of high hydrocarbon potential, leaving them in many places without well control or seismic constraints on basin architecture.

In this paper, we review evidence from a number of basins in Eurasia, where folding has been documented and alternative basin formation mechanisms such as lithospheric extension or foreland flexure cannot fully explain key features of basin geometry and evolution. We restrict ourselves to cases where independent evidence points to a major role for lithospheric folding in the basin development. We demonstrate that an interpretation in terms of folding can sometimes resolve inconsistencies resulting

Correspondence: Sierd Cloetingh, Netherlands Research Centre for Integrated Solid Earth Sciences, Faculty of Earth and Life Sciences, VU University Amsterdam, De Boelelaan 1085, 1081 HV Amsterdam, The Netherlands. E-mail: sierd.cloetingh@falw.vu.nl

from interpreting basins origin via other mechanisms. For example (Ritzmann & Faleide, 2009), the formation mechanism of intracratonic basins (ICB) is still a matter of debate. A striking feature of these basins is the prolonged intervals of low rate subsidence alternating with episodic accelerations in subsidence rates, often coeval with orogenic activity at plate boundaries. Owing to the frequent absence of evidence for thinned lithosphere below these basins, alternative models have been proposed. Stel *et al.* (1993) propose that non-extensional crustal thinning is induced by basaltic underplating, which causes thermal uplift and erosional thinning. Tectonic loading at plate boundaries is also proposed as a cause of or contributor to large-scale sag-type subsidence in plate interiors (Quinlan, 1987; Cloetingh, 1988; Leighton & Kolata, 1990) as well as phase transformations (Artyushkov, 2007). Ritzmann & Faleide (2009) point out that intraplate stresses and crustal inhomogeneities coupled with loading scenarios provide the best explanation for the Barents Sea Basin and other ICB evolution. The basins reviewed here, however, do not include cases such as the Barents Sea where the effect of stresses on topography and accommodation space has been considerably complicated by other basin formation processes.

We present inferences from thermo-mechanical models of lithospheric folding and a comparison with the results of analogue modelling of folding. We concentrate on the overall geometry of basins formed by lithospheric folding, the typical timescales intrinsic to their development and the brittle deformation patterns in the underlying lithosphere. We then discuss subsidence patterns and heat flow characteristics for such basins. We conclude by comparing key features of basin accommodation shape, vertical motions, thermal history and brittle deformation patterns of basins formed on folded lithosphere (FLB), FB, ICB, extensional basins (EB) and pull-apart basins (PAB).

LITHOSPHERIC FOLDING: AN IMPORTANT MODE OF INTRAPLATE BASIN FORMATION AND DEFORMATION

Folding of the lithosphere, involving positive and negative deflections (Fig. 1), appears to be of more importance in the large-scale deformation of intraplate domains than hitherto realized (Cloetingh *et al.*, 1999). As has been shown (Burov *et al.*, 1993; Nikishin *et al.*, 1993; Gerbault *et al.*, 1998; Cloetingh *et al.*, 1999; Schmalholtz & Podladchikov, 2000), visco-elastic folding starts to develop from the onset of compression and in contrast to elastic folding, does not require specifically large intraplate stresses. Folding may continue until the back-ground strain-rate drops, for example, due to the localization of deformation in a specific area or to reduction of far-field forces. Such intraplate deformation results from transmission of intraplate stress fields away from plate boundaries into continental forelands (Van der Pluijm *et al.*, 1997; Ziegler *et al.*, 1998; Tesauro *et al.*, 2005).

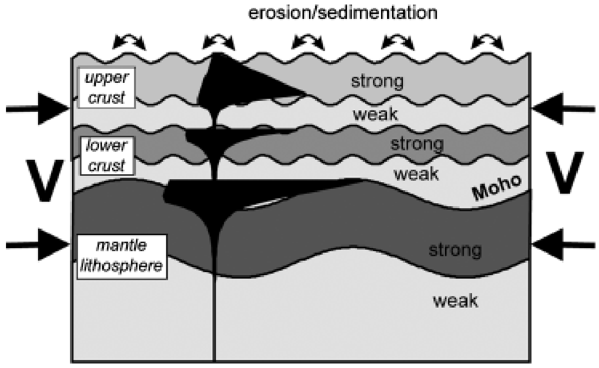

Fig. 1. Concepts of folding in rheologically stratified lithosphere and feedback with sedimentation in downfolded areas and erosion of adjacent highs. Different simultaneously occurring wavelengths of crustal and mantle folding are a consequence of the rheological stratification of the lithosphere. Surface wavelengths can be affected also by feedback with surface processes.

In continental lithosphere, several wavelengths of folding are expected to develop as a result of the presence of several rheologically competent layers decoupled from each other by weak layers (Figs 1 and 3). Crustal folding can be traced from the surface topography, neotectonic movements and free air gravity. The crust–mantle boundary (Moho) topography reflects mantle folding, because the mantle strength is highest at this interface and thus the geometry of Moho deflection is most likely to correspond to that of mantle folding. This wavelength can be traced from Bouguer gravity anomalies because the crust–mantle boundary represents also the main density contrast in the lithosphere. It is to be expected that the base of the Mechanical Lithosphere (MLB) has roughly the same geometry as the Moho deflection. Likely, the lithosphere–asthenosphere boundary (LAB) has little to do with mantle lithosphere folding except some specific cases, as the MLB (roughly corresponding to 700 °C depth) is found well above the LAB (1330 °C). Consequently, the low-viscosity zone between MLB and LAB may damp the deformation in a way that the LAB remains even flat. Owing to the low viscosity of gravitating mantle between the LAB and MLB, the LAB is not necessarily advected or down-warped with deflection of the MLB, or at least, the relations between the deformation of the MLB and LAB are not straightforward. In particular, gravity instabilities or convective movements not related to folding can perturb the LAB without impact on the MLB.

Folding has important implications for vertical motions, sedimentary basin architecture and the evolution of hydrocarbon systems (Ziegler *et al.*, 1995, 1998). The large wavelength of vertical motions associated with lithospheric folding necessitates the integration of data from large areas (Elfrink, 2001; Allen & Davies, 2007), often beyond the scope of regional structural and geophysical studies that target specific structural provinces. Recent studies on the North German Basin show neotectonic reactivation by lithospheric folding (Marotta *et al.*, 2000).

Fig. 2. Map with examples of well-documented areas affected by lithospheric folding. Areas: Central Indian Ocean Basin (CIOB) (Geller *et al*., 1983; Stein *et al*., 1989); NW European platform (Lefort & Agarwal, 1996; Marotta *et al*., 2000; Bourgeois *et al*., 2007); Pannonian Basin (Dombradi *et al*., 2010); Iberia (Cloetingh *et al*., 2002; De Vicente *et al*., 2007; Fernandez-Lozano *et al*., 2010); Central Asia (Burov *et al*., 1993; Nikishin *et al*., 1993; Burov & Molnar, 1998); Tibet/Himalayan syntaxis belt (Burg & Podladchikov, 1999; Shin *et al*., 2009); Central Australia (Lambeck, 1983; Stephenson & Lambeck, 1985); Arctic Canada (Stephenson *et al*., 1990); Transcontinental Arch of North America (Ziegler *et al*., 1995); South Caspian Basin (Guest *et al*., 2007); Laramide Foreland (USA) (Tikoff & Maxson, 2001); and Barents Sea (Ritzmann & Faleide, 2009) (map credit: NASA).

Similarly, acceleration of the Plio-Pleistocene subsidence in the North Sea Basin is attributed to stress-induced buckling of its lithosphere (Van Wees & Cloetingh, 1996). Folding of the Variscan lithosphere has been documented for Brittany (Bonnet *et al*., 2000; Lagarde *et al*., 2000), the adjacent Paris Basin (Lefort & Agarwal, 1996) and the Vosges-Black Forest arch (Dèzes *et al*., 2004; Bourgeois *et al*., 2007; Ziegler & Dèzes, 2007). Lithospheric folding, therefore, appears to be an effective mechanism for the propagation of tectonic deformation from active plate boundaries far into intraplate domains (e.g. Stephenson & Cloetingh, 1991; Burov *et al*., 1993; Ziegler *et al*., 1995, 1998).

Folding can be observed at different spatial scales. At the scale of a micro-continent that was affected by a succession of collisional events, Iberia illustrates lithospheric folding and interplay between neotectonics and surface processes (Cloetingh *et al*., 2002). An important factor favouring a lithosphere-folding scenario for Iberia is the compatibility of the thermo-tectonic age of its lithosphere and the wavelength of observed deformations.

Other well-documented examples of continental lithospheric folding occur in other cratons (Fig. 2). Prominent examples occur not only in the Western Goby area, in the Ferghana basin but also probably in the Tadjik basin of Central Asia, involving a lithosphere with thermo-tectonic ages from 150 Ma (Kazakh shield, Ferghana, Tadjik basins and likely Dzhungaria basin) to 400 Ma (Tarim basin). In this area, mantle and crustal wavelengths are 360 and 50 km, respectively, with a shortening rate of $\sim$10–20 mm year^{-1} and 200–250 km of shortening during 10–15 Myr (Burov *et al*., 1993; Burov & Molnar, 1998). Three-dimensional (3D) fold structures in the Tibetan Plateau have been inferred from GRACE satellite gravity

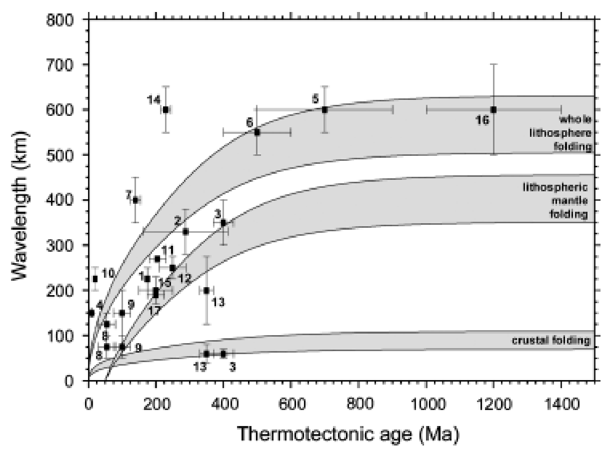

Fig. 3. Relationship between wavelengths of lithospheric folding and thermo-tectonic age of lithosphere. The grey zones correspond to theoretical folding wavelengths derived for the upper crust, mantle and coupled whole mantle folding, based on an analytical model that accounts for strength variations as a function of thermo-mechanical age (Cloetingh *et al*., 1999). Black squares are estimates for wavelengths of differential topography and thermo-tectonic ages inferred from observational studies. Numbers refer to sites listed in Table 1.

data, demonstrating prevailing fold wavelengths of 300–420 km (Shin *et al*., 2009).

The inferred wavelength of these neotectonic lithosphere folds is consistent with the general relationship between the wavelength of lithospheric folds and the thermo-tectonic age of the lithosphere shown by a global inventory of lithospheric folds (Fig. 3) (Cloetingh & Burov, 1996; Cloetingh *et al*., 2005). In some other areas of continental lithosphere folding, smaller wavelength crustal folds have also been detected (Burov *et al*., 1993; Nikishin

Table 1. Wavelengths and ages of folded lithosphere displayed in Fig. 3 (see Fig. 2 for location)

	Area	Thermo-tectonic age (Ma)	Folding wavelength, λ (km)	References
1	Tien Shan	175	200–250	Burov & Molnar (1998); Burg *et al.* (1994)
2	Western Goby	175–400	300–360	Nikishin *et al.* (1993); Burov *et al.* (1993)
3	Central Asia	370–430	50–70 (crust) 300–400 (litho-mantle)	Nikishin *et al.* (1993); Burov *et al.* (1993)
4	Himalayan syntaxis belt	8–10	150	Burg & Podladchikov (1999)
5	Central Australia	500–900	550–650	Lambeck (1983); Stephenson & Lambeck (1985); Beekman *et al.* (1997)
6	Russian platform	400–600	500–600	Nikishin *et al.* (1997)
7	South Caspian Basin	125–155	350–450	Guest *et al.* (2007)
8	Eastern Black Sea	40–80	50–100 (crust) 100–150 (litho-mantle)	Cloetingh *et al.* (2008)
9	Western Black Sea	75–125	50–100 (crust) 100–200 (litho-mantle)	Cloetingh *et al.* (2008)
10	Pannonian Basin System	20	200–250	Horváth & Cloetingh (1996); Matenco *et al.* (2007); Dombradi *et al.* (2010)
11	NW European platform	180–230	270	Bourgeois *et al.* (2007)
12	Brittany	210–290	225–275	Bonnet *et al.* (2000)
13	Iberia	330–370	40–80 (crust) 125–275 (litho-mantle)	Cloetingh *et al.* (2002)
14	Barents Sea	215–245	550–650	Ritzmann & Faleide (2009)
15	Canadian Arctic	150–250	170–230	Stephenson *et al.* (1990)
16	Transcontinental Arch of North America	1000–1400	500–700	Ziegler *et al.* (1995)
17	Laramide foreland (USA)	175–225	190	Tikoff & Maxson (2001)

et al., 1993). Thermal thinning of the mantle lithosphere, often associated with volcanism and doming, enhances lithospheric folding and appears to affect the wavelengths of folds (Burov & Cloetingh, 2009).

OBSERVATIONS

Basins developed on folded continental lithosphere have characteristic features. We illustrate this by largely concentrating on the basins of Central Asia, the folded lithosphere of Iberia, the NW European platform, the Pannonian Basin and the South Caspian Basin.

Compressional basins of Central Asia (Tienshan, Ferghana)

The young Ferghana and Tadjik basins are compressional basins northwest and north of the Pamir and south of the Tien Shan ranges (Burov & Molnar, 1998). In this area, lithosphere underwent Jurassic reactivation and is characterized by relatively young thermo-mechanical ages (175 Ma) (Burg *et al.*, 1994; Burov & Molnar, 1998). In addition to having undergone thermal weakening, the lithosphere underlying these basins also probably has a weak, quartz-dominated lower crustal rheology. This has resulted in low values for the effective elastic plate thickness (EET) of the order of 15 km (Burov & Molnar, 1998).

The Central Tien Shan consists of an alternation of ranges and basins separated by reverse faults. The Tien Shan terminates west of the right-lateral Talas-Ferghana fault by splaying into two narrow mountain chains that surround the Ferghana Valley. A narrow belt of mountains parallel to the central section of the fault slopes downwards to the Ferghana Valley, underlain by a deep basin with as much as 8 km of Cretaceous–Cenozoic sediments (Cobbold *et al.*, 1993). Gravity data suggest that the Ferghana and Tadjik basins are gravitationally overcompensated. The negative Bouguer gravity anomalies indicate a Moho several km deeper than predicted by models of local Airy isostasy (Burov & Molnar, 1998). This points to Moho down-warping due to non-isostatic processes and most probably, in this compressional context, to lithospheric folding. As demonstrated by numerical-thermomechanical experiments (Burov & Molnar, 1998), the approximately north–south shortening of the relatively thin lithosphere could have created central down-warping and anticline mountains north and south of the basin. According to this model, this shortening has produced a folding instability in the mantle lithosphere that has warped the basement immediately surrounding the basin upward, and has forced the basin floor down beneath the Ferghana Valley (with an estimate for the folding wavelength of the order of 200–250 km), possibly also producing deep mantle faulting (seen as Moho offsets in seismic reflection data).

Pre-existing thermal structure and variations in crustal thickness have played a major control on the styles and

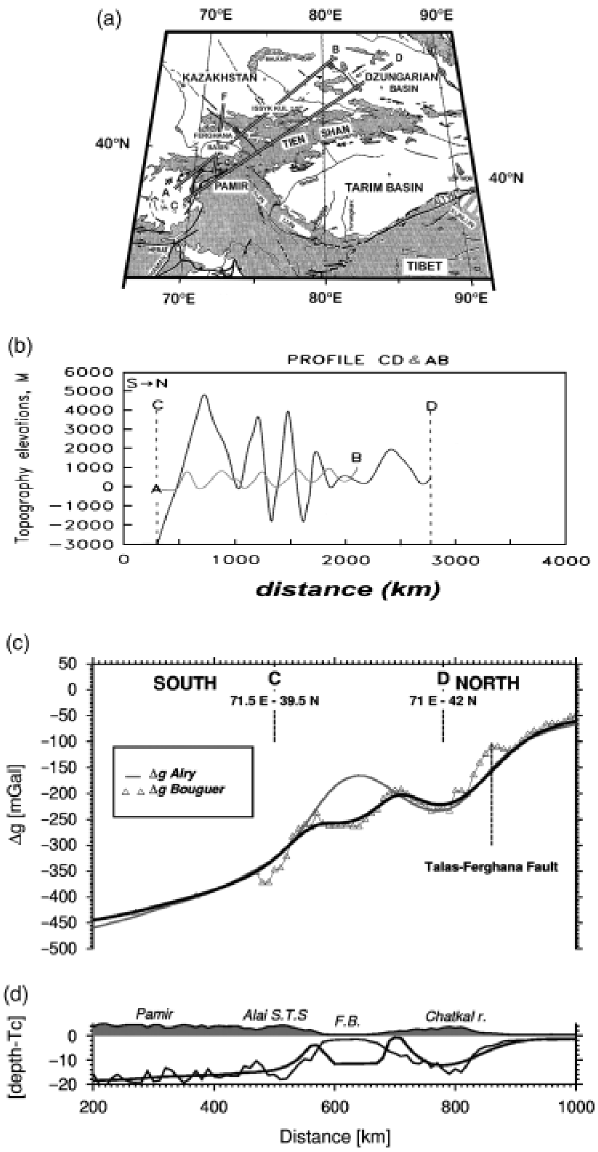

Fig. 4. (a) Map showing major tectonic features of Tien Shan area of Central Asia, with location of folding profiles discussed in Burov *et al.* (1993), Burov & Molnar (1998) and Cloetingh *et al.* (1999). (b) Neotectonic movements along the profiles AD and CD (Burov *et al.*, 1993). Modified after Cloetingh *et al.* (1999). (c) Measured and calculated Bouguer gravity anomalies for lithosphere under horizontal compression along profile F across the Ferghana basin with corresponding topography profile (after Burov & Molnar, 1998). (d) Predicted topography and Moho geometry for Airy and best fitting folding scenario. During compression, the amplitude of plate deflection changed significantly whereas the wavelength of folding stayed constant (Burov & Molnar, 1998). Fat black line is the Bouguer anomaly predicted by folding model and Moho depression, respectively. Solid grey line is Airy isostasy. Solid black line is Airy Moho. Triangles indicate observed Bouguer anomaly. Gray shaded area is topography above sea level. FB, Ferghana Basin.

distribution of faulting in this region (Fig. 4), (see also Cobbold *et al.*, 1993; Burov & Molnar, 1998). Primary faults appear before the folding develops with a spacing that is proportional to brittle layer thickness. Subsequently, the two processes, faulting and folding, co-exist in such a way that faults localize at the inflection points of folds. At this stage, the appearance of faults does not significantly influences the wavelength of folding. Because of the weakness of the lower crust, the upper crust should be completely decoupled from the mantle and interact with it only by flow in the lower crust. Lower crustal flow changes the wavelength and amplitude of the surface folding, which is terminated by the development of a single down-warped megafold (Cloetingh *et al.*, 1999). Liu *et al.* (2007) reported evidence for lithospheric folding in the Central/North China Tarim Basin region, initiated during Pliocene times, with good time constraints provided by Ar/Ar dating. Two wavelengths are found of 30 and 400 km. The thermo-mechanical age of the lithosphere is estimated to be 250 Ma, as the main thermal perturbation was associated with a major orogenic phase at 250 Ma ago. These findings are consistent with models in which decoupled lithosphere folds with 30 and 400 km wavelength correspond to, respectively, crustal and mantle folding. Deep seismic data for basins north of and within the Tibetan plateau (Li *et al.*, 2006; Liu *et al.*, 2006; Zhao *et al.*, 2006) show that folding is not limited to the Tibetan plateau (see also Shin *et al.*, 2009).

Folded lithosphere of Iberia

As reviewed by Cloetingh *et al.* (2002), Tertiary lithospheric folding of Iberia occurs in Variscan lithosphere with wavelengths of 300 km, leading to the development of a system of parallel trending basins and highs (Fig. 5a). This folding generated the distribution of basins and mountain chains, bounded by folds and faults (Cloetingh *et al.*, 2002; De Vicente *et al.*, 2007). The regularity of the fluvial network pattern of the central-western part of Iberia also indicates large-scale lithospheric folding. Alpine (mainly Cantabrian–Pyrenean related) compressional tectonics was the principal factor for closing internally drained sedimentary basins, including the Ebro, Duero and Tagus basins (Casas-Sainz & De Vicente, 2009).

A large body of geophysical and geological observations is available on the crustal geometries and stress regimes of Iberia (De Vicente *et al.*, 2007, 2008). This is supplemented by thermo-geochronology data (De Bruijne & Andriessen, 2002; Ter Voorde *et al.*, 2004), demonstrating accelerated uplift of the highs during Late Miocene–Pliocene times. In spite of the existence of recent localized volcanism in the inner part of the Iberian plate, an important contribution from thermal uplift is questionable due to the distribution of crustal thickness (Casas-Sainz & De Vicente, 2009). Fernandez-Lozano *et al.* (2010) have constructed a three-layer analogue model consisting of brittle upper crust, ductile lower crust and ductile upper mantle for Iberia. These models show that folding is associated with deformation of narrow mountain ranges separated by basins (see Fig. 5b). The narrow mountain ranges representing upper crustal pop-ups form the main topographic reliefs. Shortening is accommodated within the viscous crust beneath the pop-ups leading to lateral thickness variations of the ductile crust. These results are consistent

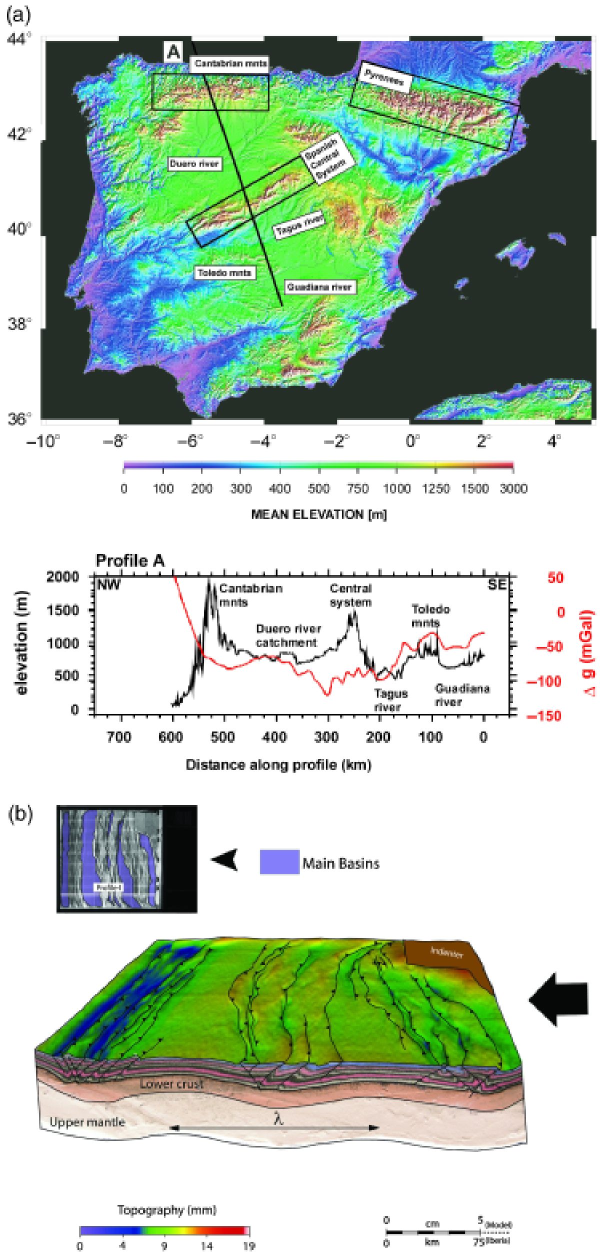

Fig. 5. First-order features of basin geometry of folded lithosphere of Iberia. (a) Topography displaying cylindrical patterns of alternating parallel trending highs and lows and corresponding gravity anomalies (red line) (see Cloetingh *et al.*, 2002). (b) Results from analogue modelling experiments, displaying pop-up structures underlying topographic highs, accompanied by folding of the Moho (Fernandez-Lozano *et al.*, 2010). Top panel shows final top view of the analogue model and location of the cross section shown below. Arrow indicates the direction of the moving wall. λ is the wavelength of folding.

with seismic and gravity data collected in the Cantabrian mountains, the Spanish Central System and the Toledo Mountains (see also Fig. 5a).

The earliest sediments in the terrestrial basins (Calvo *et al.*, 1993) were deposited during the Eocene, with very well-developed continuous successions, dominated by continental facies with high sedimentation rates. The Duero and Tagus basins began to be individualized at the onset of uplift and the formation of a topographic range in the Central System (Casas-Sainz & De Vicente, 2009). In contrast with this early more homogeneous stage, the Oligocene–Lower Miocene stratigraphy of the basins is characterized by several tectono-stratigraphic units, separated by unconformities representing short periods of time. The number and specific ages of these units vary between basins, indicating variable activity at basin borders. The fact that the largest number of breaks in the sedimentary succession is concentrated during this time interval points to a tectonic control (De Vicente & Vegas, 2009).

The final stages in the evolution of these onshore basins are characterized by widespread Miocene lacustrine sedimentation in the endorheic basins and during Pliocene and Quaternary times, by the beginning of river capture and exorheism in the Duero, Ebro and Tagus basins (Garcia-Castellanos *et al.*, 2003). Alluvial deposits were deposited by the fluvial network developed on the ancient, internally drained basins (Casas-Sainz & De Vicente, 2009). During the endorheic–exorheic transition, palaeokarstification processes and erosion occurred in the Late Miocene lacustrine limestones. Two main types of high plains can be distinguished on the Iberian Peninsula. The coupled origin of both types of surfaces can be related to uplift/sedimentation histories along the Tertiary compressional basin margins in the Iberian Peninsula (Casas-Sainz & De Vicente, 2009). The first are high plains with Tertiary sedimentary basins, containing well-preserved Late Miocene to Pliocene strata with subhorizontal bedding. Typical examples are the Duero and Tagus basins. The second consists of eroded sediments of Mesosoic and Palaeozoic rocks with planation surfaces developed on the Palaeogene–Lower Miocene ranges created by fold and thrust systems and basement uplifts. Different patterns in evolution and stratigraphy between the eastern and western Tagus basin may be related to the mechanical decoupling between Iberia and Africa during the Miocene emplacement of the Alboran Domain in the southern part of the plate. This generated extensional stresses in the eastern Iberian plate, coeval with compression and lithospheric folding in the western part of the plate (De Vicente *et al.*, 2008; De Vicente & Vegas, 2009).

In general, the dimensions of peneplains linked to EB and passive margins are larger, and their evolution involves time scales much longer than those characteristic for high plains of the Iberian plate (Casas-Sainz & De Vicente, 2009). Peneplains associated with compressional or convergent regimes (e.g. Anatolia, Central Iran and Morocco) are characterized by spatial dimensions comparable with Iberia. In addition, their tectonic setting in the hanging wall of the African–Eurasian convergence zone is also similar. Thus, the Iberian plate may be an analogue for other present-day intra-mountain basins.

The European Alpine foreland

Geophysical and geomorphological studies (e.g. Lefort & Agarwal, 1996, 2000, 2002; Marotta *et al.*, 2000) indicate large-scale compressional deformation of the European Alpine foreland lithosphere. Although different in structural grain and rheological structure (Cloetingh *et al.*, 2005; Perez-Gussinye & Watts, 2005; Tesauro *et al.*, 2007) inherited from differences in their Palaeozoic–Mesozoic history, different segments of the lithosphere in the northern Alpine European foreland share many similarities in their Cenozoic intraplate deformation. Seismic and geological evidence show that the North German Basin cannot be explained by classical models of basin formation (Marotta *et al.*, 2000). The basin underwent a polyphase history (Scheck & Bayer, 1999; Littke *et al.*, 2008) of extension in the late Triassic followed by lithospheric scale folding in the late Cretaceous–Early Cenozoic (Marotta *et al.*, 2000; Mazur *et al.*, 2005). 3D volumetric analysis shows that the compressional event was followed by faster subsidence during the Cenozoic (Scheck & Bayer, 1999). A similar observation was made by Van Wees & Cloetingh (1996) for the North Sea Basin. Lithospheric folding modified a basin formed initially by deep-seated thermal perturbations (Scheck & Bayer, 1999) with a thinned crust and shallow Moho. The Moho updoming with a high of 3 km for the height of the bulge in the southern part of the North German basin appears to be the consequence of flexural buckling of the previously thinned lithosphere by a compressive stress perpendicular to the strike of the basin.

From earliest Triassic to Late Jurassic, the Paris Basin (Fig. 6a) subsided in an extensional framework and was larger than the present basin (Guillocheau et al., 2000). The western margin of the Paris Basin and the rifted Atlantic margin of France were subject to thermal rejuvenation during Mesozoic extension related to North Atlantic rifting (Robin *et al.*, 2003; Ziegler & Dèzes, 2006). Subsequent compressional intraplate deformation (Ziegler *et al.*, 1995) also affected the Paris Basin (Lefort & Agarwal, 1996). Numerical modelling indicates that the amplitude of the compression-induced vertical deflection in the Paris Basin is relatively small, requiring additional mechanisms such as flexure due to the load by the Alpine system (Bourgeois *et al.*, 2007; Ziegler & Dèzes, 2007). However, periodic deformation at the same wavelength occurs northwest of the Paris Basin (Fig. 6a, Bourgeois *et al.*, 2007), which would not be the case if the north-eastern part of the basin was flexed down by the load of the Alps. Bourgeois *et al.* (2007) carefully analysed basement geometry and timing of vertical motions in the NW European platform. They separate the contributions from the European Cenozoic Rift System (ECRIS) and the contributions from long-wavelength folding striking NE and located between the Alpine front and the North Sea. According to their analysis, the ECRIS developed mostly between 37 and 17 Ma, whereas lithospheric folds developed between 17 Ma and present, with a wavelength of 270 km and amplitude of 1500 m (see Fig. 6b).

Quaternary folding of the Variscan lithosphere in the area of the Armorican Massif (Bonnet *et al.*, 2000) developed folds with a wavelength of 250 km, pointing to a mantle-lithospheric control on deformation. The timing and spatial pattern of uplift inferred from river incision studies in Brittany are incompatible with a glacio-eustatic origin. Therefore, Bonnet *et al.* (2000) related the vertical motions to deflection of the lithosphere by the present-day NW–SE directed compressional intraplate stress field. Stress-induced uplift of the area appears to control fluvial incision rates and the position of the main drainage divides. Leveling studies (LeNotre *et al.*, 1999) indicate its ongoing deformation.

Pannonian basin system

Recent studies of the Pannonian Basin system – formed as a Miocene back-arc basin behind the Carpathian arc – show that active crustal deformation resulted in significant differential vertical motions during Late Neogene times (Horváth & Cloetingh, 1996; Cloetingh *et al.*, 2005, 2006; Horváth *et al.*, 2006; Matenco *et al.*, 2007; Fig. 7a). The river network in the area is affected by differential neotectonic crustal motions (Necea *et al.*, 2005; Dombradi *et al.*, 2010).

The Late Neogene evolution of the Pannonian Basin is largely controlled by its interaction with the Carpathian arc and the Adriatic indentor impinging the Pannonian basin lithosphere (e.g. Bada *et al.*, 2001). As a result of the consumption of subductable lithosphere of the European foreland, the Pannonian basin became locked. At the same time, the continuous N–NE directed indentation of the Adriatic microplate built up a high level of compressional stresses in the Pannonian Basin. The structural inversion of the basin is a direct consequence of the temporal changes in the stress field from extension to compression. Recent studies of the stress field together with an extensive array of geological and geophysical data have shown that horizontal stresses are transmitted from the plate boundaries into the interior of the Pannonian Basin (Bada *et al.*, 2007).

The Pannonian Basin is underlain by what is probably the hottest lithosphere of continental Europe, characterized by a very low lithospheric strength (Tesauro *et al.*, 2007). Miocene extension resulted in a high level of mantle stretching, leading to a strength distribution with practically zero strength in the subcrustal lithosphere and lower crust (Cloetingh *et al.*, 2005), making it prone to tectonic reactivation. Therefore, in this area relatively low compressional stresses induced mainly by plate boundary interactions, and further amplified by topography-induced stresses (Bada *et al.*, 2001), could initiate significant intraplate deformation.

It should be noted that in the Pannonian basin system, seismic tomography (Wortel & Spakman, 2000) supports slab detachment under the adjacent Romanian Carpathians. At the same time, the seismic tomography shows the presence of a hot upper mantle below the folded lithosphere in the Pannonian basin. In this area, therefore, the upper mantle structure reflects more the back-arc extension before the folding than the consequences of folding on the density stratification of the mantle. The reverse is true for the crustal configuration. The geometries imaged by the crustal scale deep seismic reflection profiling are clearly dominated by compressional structures resulting from folding (Fig. 7b).

Quaternary patterns of differential uplift and subsidence with a timing coeval with an increased level of compressional stresses are interpreted as caused by

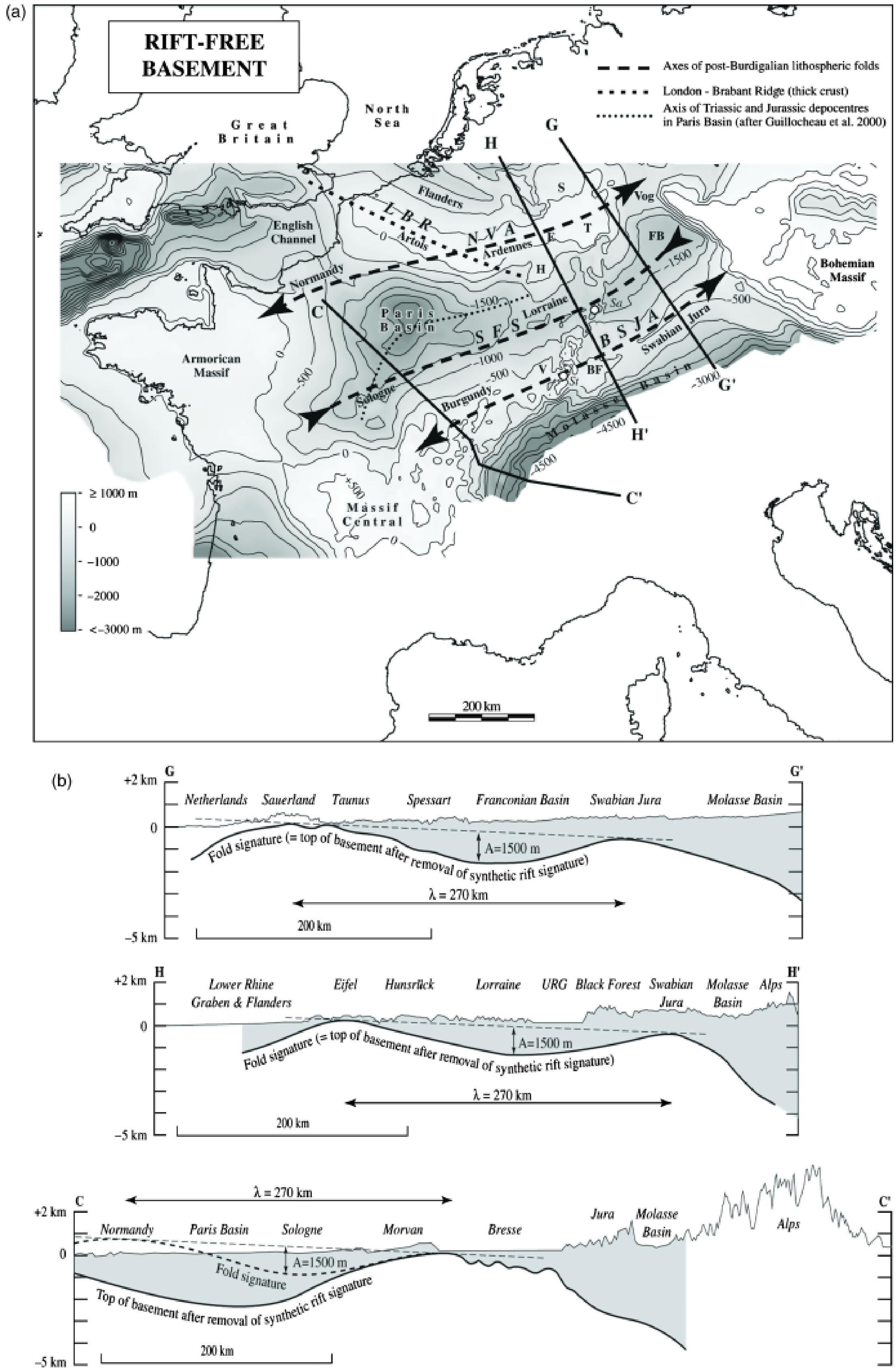

lithospheric folding (Horváth & Cloetingh, 1996; Cloetingh *et al.*, 2006; Horváth *et al.*, 2006; Bada *et al.*, 2007). Late-stage compressional deformation of the Pannonian basin is demonstrated to be of key importance for the geometry of basin fill (Sacchi *et al.*, 1999, see Fig. 7b) and for its reservoir structures, both crucial in assessment of its hydrocarbon potential (Horváth, 1995). Analogue tectonic experiments by Dombradi *et al.* (2010) further examine accumulation and transmission of stresses in the hot and weak back-arc lithosphere of the Pannonian basin and the interplay between lithospheric processes and the intrabasinal topography development. Based on available rheological and seismotectonic constraints, the basin system is represented by a two-layer model with a 10–15 km thick brittle upper crust. The lower crust and the mantle are represented by a low-strength layer of 45 km thickness (Dombradi *et al.*, 2010). The strain rates applied were constrained by GPS velocities (Grenerczy *et al.*, 2005). In the experiments, lithospheric folds develop with wavelengths equivalent to 200–250 km (Fig. 7c). The experiments also show that crustal thickness variations largely determine the localization of stresses. Topographic profiles extracted by laser scans of the model show that surface topography reflects long wavelength buckling of the lithosphere. These results are compatible with Pliocene–Quaternary subsidence, which occurs in the centre of the Pannonian basin, simultaneously with an accelerated uplift at the basin margins. The latter has lead to elevated topography of up to 1 km in areas at the rim of the Pannonian Basin such as the Styrian, Zala and Transylvanian basins (Cloetingh *et al.*, 2006).

The South Caspian Basin

The South Caspian Basin with an estimated sedimentary thickness up to 20 km (Brunet *et al.*, 2003; Egan *et al.*, 2009), is probably one the deepest basins in the world. It is flanked by the Alborz Mountains to the south, with an elevation of 2–4 km (see Fig. 8). The transition between basin and flanking high is abrupt and coincides with a coastline bounded by a major fault system. The formation of the South Caspian Basin is enigmatic. Attempts to explain it as an EB or as a FB have been unsuccessful. There is a lack of evidence for basin extension and both stretching models and topographic loads and slab pull operating on down flexed lithosphere in FB systems cannot explain differential vertical motions of this order of magnitude. As a result, phase changes in continental crust have been proposed as a mechanism for the formation of this superdeep basin (Artyushkov, 2007). A limitation in conclusively resolving the basin formation mechanism is the lack of multichannel seismic reflection data capable of imaging crustal structure below the thick sedimentary sequences. Over the last few years, however, other constraints on the area have become available (e.g. Guest *et al.*, 2007).

Figure 8 presents a cross section of northern Iran and the South Caspian Basin (Guest *et al.*, 2007). As shown, wavelengths for compressional folding of the lithosphere are typically in the range of 400 km. Although the actual basin formation mechanism for the Caspian Basin is not well resolved (e.g. Artyushkov, 2007), late Neogene folding has been affecting a lithosphere probably thermally reset by middle Late Jurassic marginal basin formation (Guest *et al.*, 2007) with a thermo-mechanical age at the onset of collision of 130–150 Ma. Satelite data demonstrate an exceptionally large gravity anomaly over the basin (Kaban, 2002). Seismic tomography shows slab detachment under the Iranian plateau (Hafkenscheid *et al.*, 2006; Alinaghi *et al.*, 2007) beginning at about 10–15 Ma.

Basin analysis has shown that basement inversion has occurred 20 Ma ago, simultaneously with the slowing of Arabian/Eurasian plate convergence and the onset of accumulation of Neogene clastics in FB (e.g. Fakhari *et al.*, 2008). By 10 Ma, contraction occurred by underplating of the Arabian crustal units beneath the Iranian plate. Estimated shortening rates from current geodetic surveys (Vernant *et al.*, 2004) are 7 mm year^{-1}. Results from geothermochronology demonstrate rapid uplift of the Alborz mountains, with rates of 0.7 km Myr^{-1} exhumation between 6 and 4 Ma (Axen *et al.*, 2001), implying approximately 10 km of uplift. This uplift was nearly synchronous with rapid South Caspian subsidence (Nadirov *et al.*, 1997) and subsequent folding (Devlin *et al.*, 1999). South Caspian sedimentation rates locally increased more than 10-fold at *ca*. 6 Ma, with more than 10 km of sediments deposited since then. Axen *et al.* (2001) argue that if approximately 10 km of post 6 Ma sediments are present in this basin, then as much as 20 km (equivalent to 80%) of the structural relief of about 25 km between the high Alborz and the southernmost Caspian basement may be younger than 6 Ma.

Folds in the southernmost Caspian Basin (Devlin *et al.*, 1999) and in the Neogene of the Northern Alborz foothills imply contraction. The lack of a crustal root under the Alborz Mountains also points to a flexural support by the South Caspian basement (Axen *et al.*, 2001). The simulta-

Fig. 6. (a) Map of elevation of basement in the NW Alpine foreland with rift signature removed from the map of actual basement (from Bourgeois *et al.*, 2007). Dashed lines show axes of Late Neogene lithospheric folds, with a succession of anticlines and synclines: the Normandy–Vogelsberg anticline (NVA), Sologne–Franconian Basin Syncline (SFS) and the Burgundy–Swabian Jura Anticline (BSJA). LBR, London Brabant Ridge with thick crust; BF, Black Forest; FB, Franconian Basin; E, Eifel; H, Hunsruck; S, Sauerland; T, Taunus; V, Vosges. (b) Cross sections of top basement in the NW Alpine foreland with rift signatures removed (Bourgeois *et al.*, 2007; see for location Fig. 6a). Thin line: actual topography surface. Bold line: elevation of top basement as predicted in the absence of rifting. Fold signatures are similar with a wavelength λ of 270 km and amplitude A of 1500 m in the Franconian Basin (cross-section G-G′) and in the upper Rhine Graben area (cross-section H-H′). In the Paris basin, development of folds with assumed same wavelength and amplitude (stippled bold line in cross-section C-C′), implies subsidence of Sologne and uplift of Normandy.

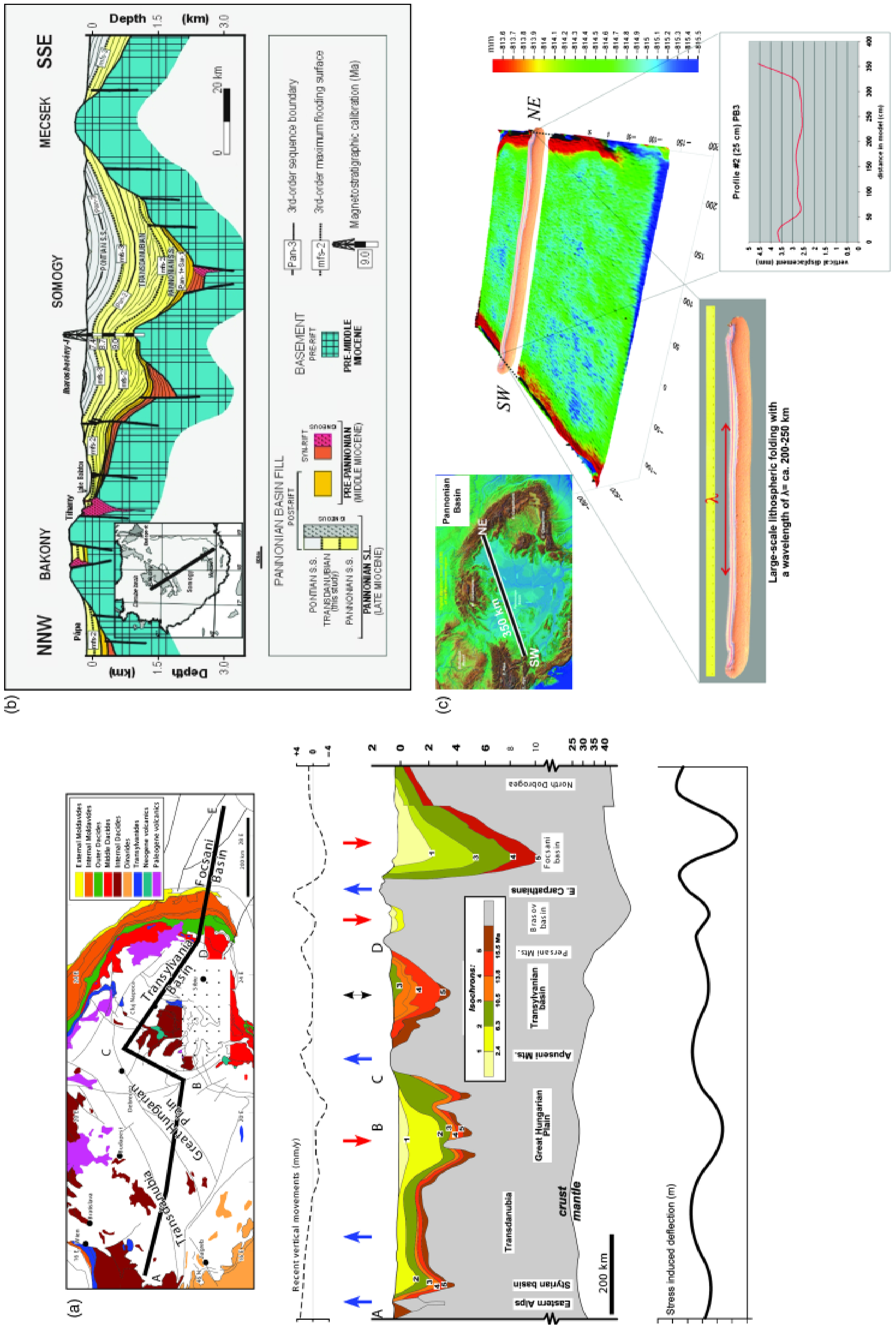
(a)
(b)
(c)
NNW
SSE
BAKONY
SOMOGY
MECSEK
Depth (km)
20 km
PANNONIAN BASIN FILL
BASEMENT
3rd-order sequence boundary
3rd-order maximum flooding surface
Magnetostratigraphic calibration (Ma)
SW
NE
Pannonian Basin
350 km
Profile #2 (25 cm) PB3
Large-scale lithospheric folding with a wavelength of λ= ca. 200-250 km
Transylvanian Basin
Focsani Basin
Great Hungarian Plain
Transdanubia
Recent vertical movements (mm/y)
Isochrons:
crust
mantle
200 km
Stress induced deflection (m)

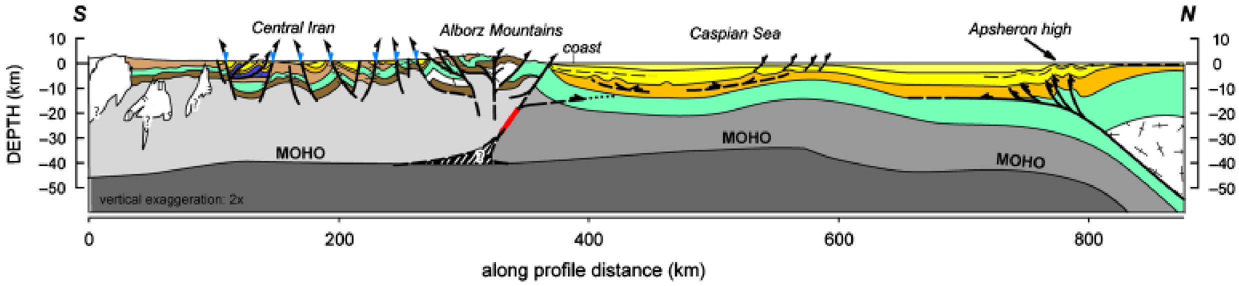

Fig. 8. Schematic north-south trending cross section illustrating the basic tectonic setting for northern Iran and the South Caspian Basin (Guest *et al.*, 2007), illustrating basin inversion of the central Iranian basin, pronounced differential topography at the transition of the Alborz mountains, with a topographic high of several km's and the South Caspian Basin with about 20 km of sedimentary infill.

neous reversal of Zagros strike slip and extrusion of central Iran, coarse Zagros molasse deposition, Dead Sea transform reorganisation, Red Sea oceanic spreading (Chu & Gordon, 1998) all initiated around 5 ± 2 Ma (e.g. Axen *et al.*, 2001; Smit *et al.*, 2010), was interpreted by these authors in terms of a widespread tectonic event. Slab detachment could explain part of the recent uplift of Iran, but does not directly explain the simultaneous dramatic subsidence in the adjacent Caspian Basin. However, slab detachment could have an indirect effect if reducing slab pull forces acting on the downgoing lithosphere promote the development of compressional stresses in both the downgoing and overriding plates (Cloetingh *et al.*, 2004; Matenco *et al.*, 2007).

Guest *et al.* (2007) argue in favour of compressional deformation of the South Caspian Basin/Alborz mountains. This interpretation was largely based on available industrial seismic reflection data and gravity data for the basin and followed a similar proposition made for the late-stage deformation of the adjacent Black Sea (Nikishin *et al.*, 2003; Cloetingh *et al.*, 2008). Guest *et al.* (2007) present kinematic models, without addressing the reason for the difference in the order of magnitude of the basin depression and the adjacent high. Analogue experiments (Sokoutis *et al.* 2005) show that when compression acts on two blocks with contrasting thickness (and rigidity), a major syncline will develop on top of the suture zone separating these blocks, flanked by an anticline of much lower amplitude. These results are consistent with predictions from folding theory that as a result of the acting gravity field, downwarping is mechanically more effective than up-warping against the action of gravity forces. The presented numerical experiments illustrate this (see for example Fig. 9).

Basins on folded lithosphere in Eurasia: differences and similarities in lithospheric deformation and basin habitat

Comparison of lithospheric deformation in Central Asia, Iberia, the NW European Alpine foreland, the Pannonian Basin and the South Caspian Basin demonstrates common features compatible with an interpretation in terms of basins developed on folded lithosphere. Among these are their symmetrical shape, dimensions and the temporal association of their basin formation history with the build up of intraplate stresses. Important differences can be observed between the Central Asian and Iberian basins and the South Caspian Basin on one side and the European Alpine foreland and the Pannonian Basin on the other side.

The Central Asian Basins and the basins of the Iberian plate were initiated by Tertiary folding, whereas the European Alpine foreland underwent a polyphase history, following Carboniferous and Triassic stretching (Scheck & Bayer, 1999; Le Solleuz *et al.*, 2004), before Late Cretaceous–Early Cenozoic folding. Similarly, the Pannonian Basin, formed by back-arc extension in Miocene times, was subsequently compressionally reactivated (Cloetingh *et al.*, 2008). The origin of the South Caspian Basin is not well resolved, but km scale vertical motions are compatible with a megafold as a prime control on present-day basin geometry. These differences in evolution have a pronounced impact on basin dimensions and on the nature of basin fill. The Central Asian basins, the folded basins of Iberia and the South Caspian Basin have a wavelength compatible with theoretical predictions. In contrast, the fold wavelengths of the European Alpine foreland and the Pannonian Basin appear to be primarily controlled by the pre-existing

Fig. 7. (a) Schematic E-W cross section through the Pannonian–Carpathian basin system (Cloetingh *et al.*, 2008), displaying anomalous Late Neogene acceleration of the subsidence between isochrons 2 and 0 Ma in the centre of the Pannonian basin and the Focsani depression of the Southern Carpathian foredeep, flanked by uplifting highs. Wavelengths of the differential vertical motions are typically of the order of 250 km. (b) Interpreted seismic section in the central part of the Pannonian Basin (Sacchi *et al.*, 1999) showing evidence for late Neogene crustal scale folding at scales of 20–40 km. Note syn-rift grabens formed during the Miocene back-arc extension of the basin. (c) Results of analogue tectonic experiments carried out to examine the patterns of differential vertical motions in the northern part of the Pannonian Basin and surrounding areas (Dombradi *et al.*, 2010), demonstrating atypical folding of variable amplitude with a wavelength equivalent to 200–250 km.

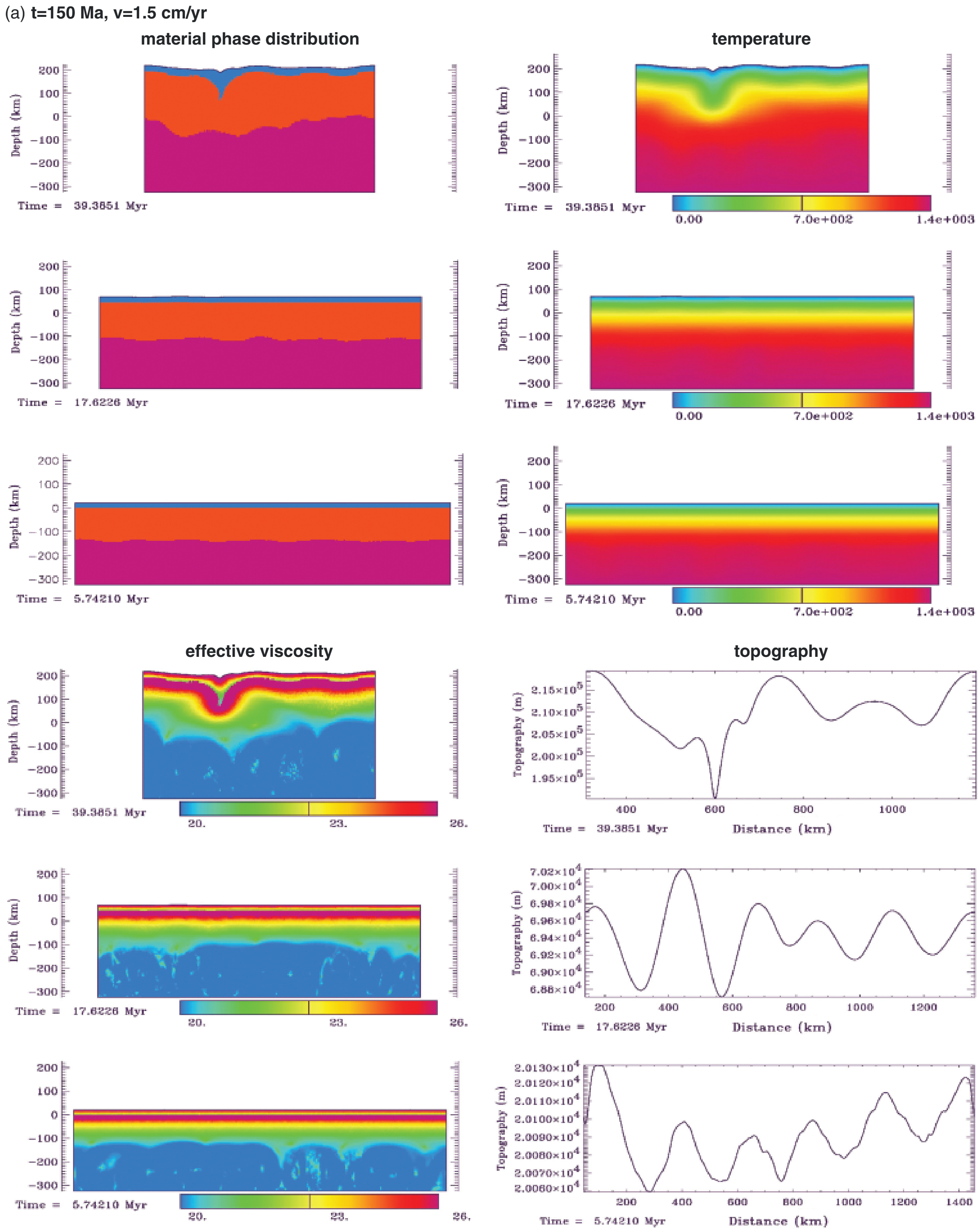

Fig. 9. Characteristic patterns of continental lithosphere deformation induced by folding of the lithosphere with time. Increasing amounts of horizontal shortening for a 150 Ma old lithosphere with convergence rates of (a) 1.5 cm year^{-1} and (b) 3 cm year^{-1}. From left to right: material phase distribution (with blue for the crust, orange for the mantle lithosphere and red for the upper mantle below the lithosphere), temperature, effective viscosity and topography.

geometry of the sediment–basement interface and pre-existing Moho topography inherited from the pre-folding stage. Differences occur also in the development of the ranges flanking the basins. In Central Asia and Iberia, these highs have amplitudes and widths comparable with the prediction for periodic folding, whereas in the Paris Basin and the North German Basin these highs are less well developed. The ratio of the depth of the South Caspian Basin to the height of the flanking Alborz Mountains is compatible with a megafold under this area of dramatic differential

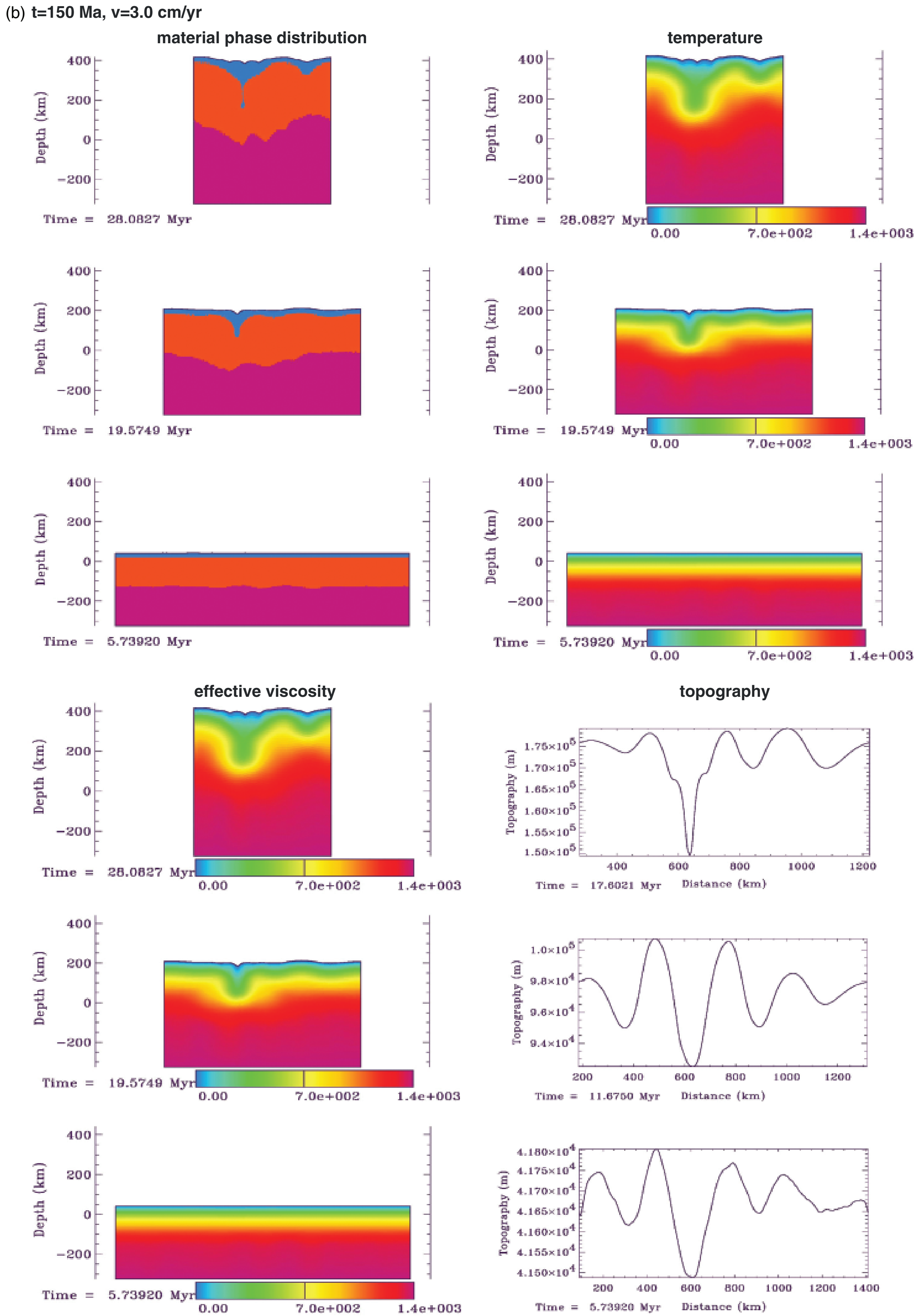

Fig. 9. Continued.

topography. The large amplitudes of folding at the flanks of the Pannonian Basin system are compatible with its extremely weak rheology. Differences in the amplitude of the highs might also partly result from the differences in neotectonic shortening. The highs bounding the basins of Iberia, Pannonian Basin, South Caspian Basin and Central Asia, located relatively close to the site of ongoing convergence, are still experiencing active uplift. This is much less the case for the low strain-deforming areas of the NW European platform and the North German basin where the peak compression occurred during Late Cretaceous–Early Cenozoic. Another difference occurs in the depositional regime prevailing in these basins. The closed basin systems of Central Asia, Iberia and the intra-Carpathian Pannonian Basin are dominated by continental and lacustrine deposits, whereas capture is usually a late-stage feature of these basins. The Paris basin of the NW European platform has a basin fill largely dominated by marine sediments deposited during the pre-folding stage of their evolution, followed by marine Tertiary successions in the basin centre with truncated basin margins. The creation of basin highs in this case was in general not capable of interrupting open connections to marine environments.

A general observation for all these basin systems is the flatness of sedimentary sequences in the depocentres. Faulting plays a minor role in the basin development. Faulting appears to be concentrated at the basin margins, with a highly variable depth extent, varying from upper crustal scale faults bounding pop-up structures in the Central System of Iberia and the Pannonian Basin to minor faulting in the basement of the North German Basin. The thermal regimes of the basins are similar with thermal histories strongly affected by subsidence and sediment deposition on down flexed lithosphere, pre-conditioned by its thermo-mechanical age.

THE ROLE OF LITHOSPHERIC RHEOLOGY

Folding is commonly associated with periodic deformation of layered structures with contrasting mechanical properties. As a consequence, the harmonic spatial periodicity is often believed to be its primary, almost synonymous, identifying factor. However, from a mechanical point of view, constant wavelength is not a necessary requirement. Folding is a compressional instability developing in stiff layers embedded in a weaker material. The harmonic solution of the equilibrium and conservation equations is a possible solution (Burov & Molnar, 1998; Muehlhaus *et al.*, 1998; Cloetingh *et al.*, 1999). The physical mechanism of folding is well understood. In a continuous layered medium, the stresses and strains must be continued across the interfaces between the layers. In multi-layer systems with contrasting mechanical properties (e.g. strong and weak layers), this requirement may be difficult to satisfy, because the same amount of shortening in a stiffer layer would require much larger stress than in the neighbouring weaker layer. The system becomes unstable, and in attempting to reduce the stress and strain unconformities at the interfaces between the layers, starts to fold (or buckle) in response to very small perturbations. In non-elastic media with strain-dependent properties, locally increased flexural strain at the fold limbs can create weakened zones that significantly facilitate further deformation. These weak or softened plastic or viscous zones are often referred to as inelastic hinges, because the system easily folds at such weakened zones. Homogeneous shortening of the lithosphere under horizontal compression requires more work than required by an equivalent amount of shortening by folding. However, shortening by underthrusting/subduction of the lithosphere may be more mechanically efficient than folding but may be blocked or unable to start immediately after the onset of shortening. For this reason, folding is likely to be a primary and common response to tectonic compression. Folding probably may continue, in an attenuated form, even after the beginning of subduction (Cloetingh *et al.*, 1999), or re-appear when the subduction channel is locked or during the aftermath of collision (Cloetingh *et al.*, 2004; Matenco *et al.*, 2007).

The rheological structure of the lithosphere (Watts & Burov, 2003) is a key factor in lithospheric folding. Compressional stresses must build up to a level comparable with the integrated strength of the lithosphere in order to induce folding. Before the advent of rheological models based on extrapolation of laboratory experiments (Goetze & Evans, 1979; Carter & Tsenn, 1987), lithospheric stresses were thought to be incapable of reaching the failure levels required for folding (Turcotte & Schubert, 2002).

The simplest expression of the folding process is in oceanic lithosphere, characterized by an absence of a rheological stratification, and with thermo-mechanical ages spanning a limited age window with a maximum of 200 Myr (Geller *et al.*, 1983; N. Zitellini *et al.*, unpublished data). Because weak lithosphere is easier to fold than strong lithosphere, one would expect the first observations of lithospheric folding from the rheologically weak continental plate interiors. However, the observation of folding of the relatively strong lithosphere of the central Indian Ocean with a thermo-mechanical age of 80 Ma and with wavelengths of 200–250 km (Geller *et al.*, 1983; McAdoo & Sandwell, 1985; Stein *et al.*, 1989; Bull & Scrutton, 1992) triggered the interest in this mode of deformation. There may be two reasons for this. First, the recognition of folding, by mapping of basin reflectors and gravity anomalies requires spatial scales of several hundreds of kilometres. This is feasible with marine geophysical surveys, but generally in excess of the spatial scales covered by land surveys. An exception has been the systematic mapping of basins in Central Australia, located on strong lithosphere with a thermo-mechanical age of approximately 700 Ma (Lambeck, 1983; Stephenson & Lambeck, 1985). The Indo-Australian plate is under an exceptionally high level of compression (Stein *et al.*, 1989), as a result of its collision with the Eurasian plate. Under these conditions, high stresses might have been more important than the rheology of the plate interior (Beekman *et al.*, 1996; Gerbault *et al.*, 1998; Gerbault, 2000).

Secondly, folding in oceanic lithosphere is not affected by surface erosion, making it relatively easy to recognize. The presence of only one dominant folding wavelength characteristic of non-stratified oceanic lithosphere also facilitated a quantitative interpretation. Following the early studies in the Indian Ocean and in Central Australia in the rear of the Indian–Eurasian collision, attention shifted to the other side of the plate contact in Central Asia. Large-scale folding patterns were recognized through analysis of geophysical data, including gravity and topography (Burov *et al.*, 1993; Nikishin *et al.*, 1993; Burov & Molnar, 1998) as well as detailed geological studies (Cobbold *et al.*, 1993).

On the basis of an inventory of currently available results of studies of folded continental lithosphere, it appears that in general the observed wavelengths of folding follow theoretical predictions for wavelengths as a function of thermo-mechanical age remarkably well (see Fig. 3).

NUMERICAL EXPERIMENTS FOR SELECTED THERMO-MECHANICAL AGES OF LITHOSPHERE

Folding is an unstable deformation that may develop in stratified media with significant competence contrasts, as occurring in the continental lithosphere, in response to horizontal loading (Biot, 1961; Ramberg, 1961). These instabilities may develop under compression or basal shear as a result of strain/stress incompatibility on the interfaces between layers of different competence. In the initial stages of deformation, compressional instabilities cause periodic folds with an exponential growth rate and a dominant wavelength λ roughly proportional to five to ten times the thickness(es) of the competent layer(s). In the lithosphere, the layer thickness is that of the competent core h. Hence, $h = 10$–100 km gives rise to $\lambda = 50$–1000 km.

'Biot's', or linear, folding encompasses the cases where compression of the lithosphere occurs from the beginning, leading to the formation of alternating (synclinal) basins and (anticlinal) highs, and where the conditions of the linear theory are more or less satisfied (e.g. thin layer approximation, no strain-softening, plane layers). For linear folding in a Newtonian medium, an asymptotic relationship derived from the thin layer equilibrium equation is (Biot, 1961; Ramberg, 1961):

$$\lambda_1 = 2\pi h(\mu_{l1}/6\mu_{l2})^{1/3} \tag{1}$$

where λ_1 is the 'Laplacian' dominant wavelength of folding in the absence of gravity, h is the thickness of the competent layer (crustal or mantle) and μ_{l1} and μ_{l2} are the effective viscosities (or competencies) of the strong layer and weak surrounding material, respectively. The above equation, derived assuming zero gravity, provides estimates of $\lambda_1/h = 20$–40 for typical competence contrasts. This does not hold for most lithospheric-scale cases, where $\lambda/h = 4$–6 is more common due to the influence of the gravity-dependent terms. A reduction of the normalized characteristic wavelength to values around 4 is also predicted for power-law rheology or plastic layers (Smith, 1979). For a single stiff viscous layer on top of an inviscid medium, the dominant gravity-dependent wavelength is (Burov & Molnar, 1998):

$$\lambda_g \sim 2\pi[2h\dot{\varepsilon}\mu_{\mathrm{eff}}/(\Delta\rho g)]^{1/2} \tag{2}$$

where $\Delta\rho$ is the density contrast, $\dot{\varepsilon}$ is the strain rate, μ_{eff} is the layers' effective ductile viscosity (see Appendix A), n is the power-law exponent and h is the thickness of the competent layer.

At large amounts of shortening, this deformation may become aperiodic, (Hunt *et al.*, 1996) so that the wavelength and amplitude of folding vary along the deformed transect. Plume-induced periodic deformation (Burov & Cloetingh, 2009) also includes folding or boudinage caused by shear on the base of the lithosphere. However, the prime cause for folding of continental lithosphere is tectonic loading by horizontal far-field forces. For characteristic parameters of various layers within the continental lithosphere ($h = 10$–120 km, $\mu = 10^{19}$–10^{26} Pa s: $\Delta\rho = 10$–600 kg m^{-3}), Eqns (1) and (2) predict folding wavelengths that may vary from 30 km (upper crustal folding) to as high as 600–800 km. The findings of numerical models (Cloetingh *et al.*, 1999) are in excellent agreement with analogue tectonic experiments (Sokoutis *et al.*, 2005). Numerical experiments show that the wavelength and amplitude of folding are largely controlled by the thermo-mechanical age and less by the rate of shortening (Burov & Cloetingh, 2009). Lithospheres older than 500 Ma develop nearly the same wavelength of folding as 1000-Ma-old lithosphere because of the similar nearly stationary thermal state. Here, therefore, we restrict ourselves to a set of experiments for ages of 150 and 300 Ma and convergence rates of 1.5 and 3 cm year^{-1}.

Surface topography and sedimentary deposition are described through diffusion-like erosion laws and fluvial transport laws (Gossman, 1976; Kirkby, 1986; Leeder, 1991; Beaumont *et al.*, 1992; Kooi and Beaumont, 1994):

$$\mathrm{d}h/\mathrm{d}t = \mathrm{div}[k^*(x, h, \nabla h)\nabla h]$$

where h is the topography, t is the time, x is the horizontal coordinate and k^* is an experimentally established scale-dependent coefficient of erosion (500–1000 m^2 year^{-1}). For simplicity, we used zero-order linear diffusion (k^* constant) for the short-range erosion and flat deposition for long-range fluvial transport (Avouac & Burov, 1996). The hill-slope erosion law ensures conservation of matter but holds only for small scales. At large scales, it is no longer applicable, and conservation of matter is not observed, because some sediments are lost due to transport out of the system by long-range processes.

Figure 9 shows the results of the experiments for relatively young (150 Ma) lithosphere compressed at rates of 1.5 and 3 cm year^{-1}. Strongly decoupled low-amplitude short wavelength (mantle wavelength $\lambda = 250$ km) folding developed leading to crustal thickening above a synclinal

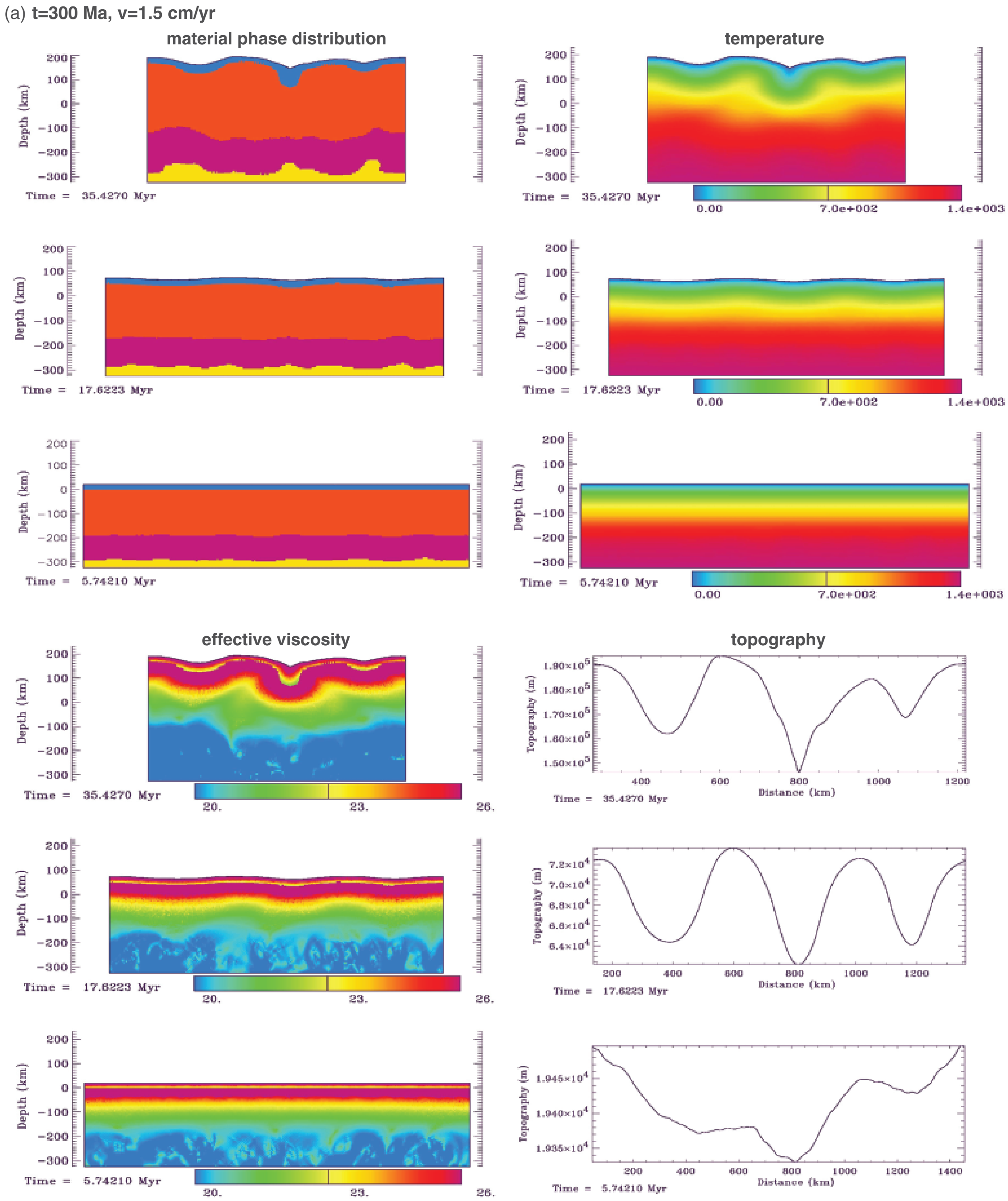

Fig. 10. Characteristic patterns of continental lithosphere deformation induced by folding of lithosphere with time. Increasing amounts of horizontal shortening for a 300 Ma old lithosphere with convergence rates of (a) 1.5 cm year^{-1} and (b) 3 cm year^{-1}. From left to right: phase distribution, temperature, effective viscosity and topography.

mantle fold. At later stages, harmonic folding was followed by mega-folding (Burg & Podladchikov, 1999; Cloetingh *et al.*, 1999). For higher rates of shortening, these mantle synclines developed in a mode resembling symmetric subduction. For lower convergence rates (Fig. 9a), folding does not develop due to the low Peclet number of the system, leading to heat diffusion and weakening of folds.

Folding is well developed for medium (300 Ma) age lithosphere (Fig. 10). This case is characterized by long mantle wavelengths ($\lambda = 360$ km) and high surface amplitudes (2000 m after 10 Myr). These compare well with observations from Iberia (Fernandez-Lozano *et al.*, 2010), Western Goby and the Ferghana basin in Central Asia (Burov *et al.*, 1993; Burov & Molnar, 1998). At late stages

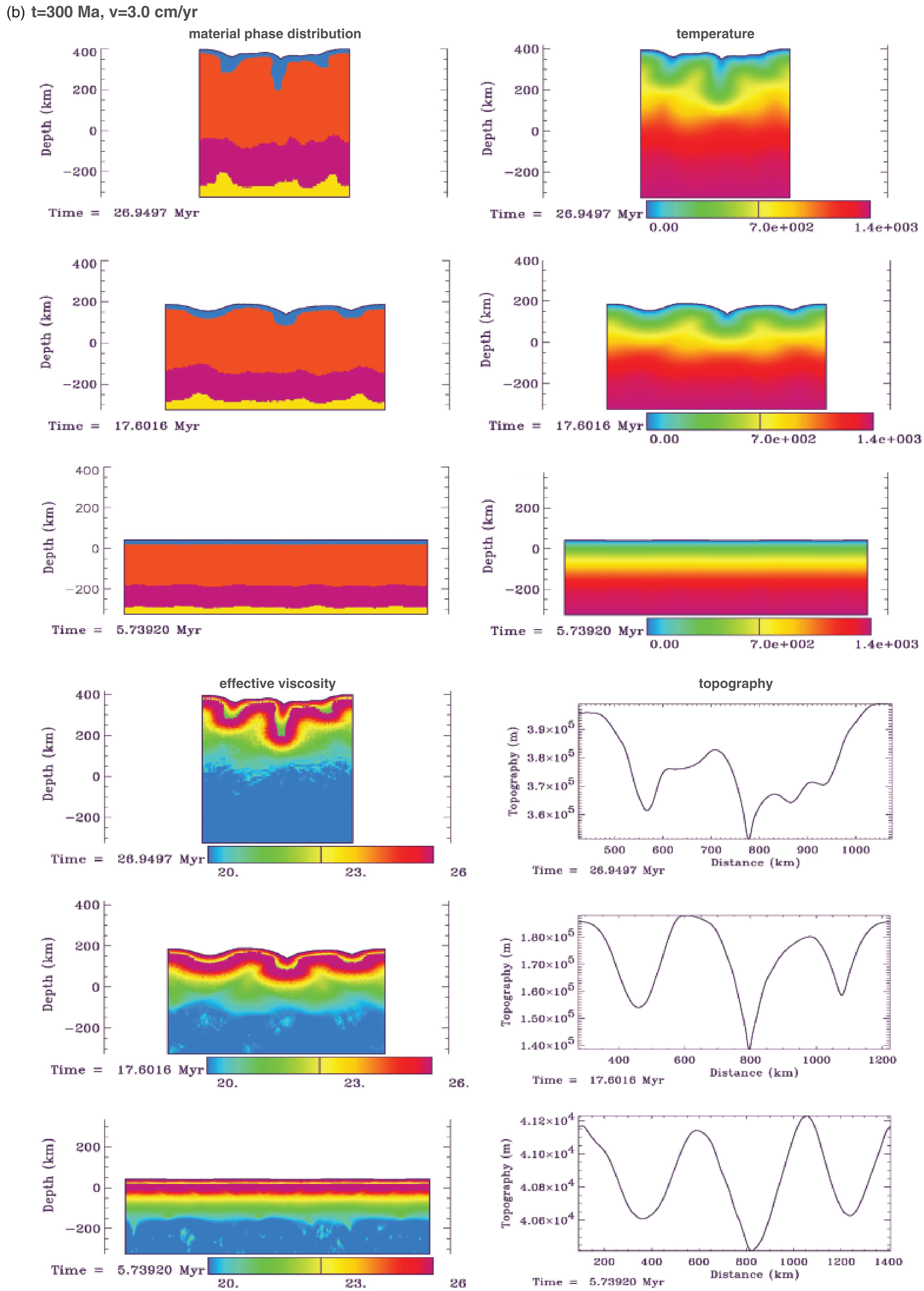

Fig. 10. Continued.

(10–26 Myr since the onset of shortening for 3 cm year^{-1} or 20–50% of shortening), folding becomes aperiodic, leading to mega-folding (Burg & Podladchikov, 1999; Cloetingh *et al.*, 1999) and the subsequent formation of high-amplitude crustal down-warps. The amplitude of vertical movements may reach 20 km ($\pm$ 10 km) or even more. As pointed out earlier, such high amplitudes of vertical motions are observed in the South Caspian Basin (Guest *et al.*, 2007) and the Barents Sea (Ritzmann & Faleide, 2009). However, it may be relatively rare for folding to continue for periods in excess of 10 Myr. More typically is that at a certain stage deformation localizes along single major fault zones (Cloetingh *et al.*, 1999; Gerbault *et al.*, 1998).

As was discussed by Bird (1991), Avouac & Burov (1996) and Cloetingh *et al.* (1999), large-scale undulations of the lithosphere cannot be preserved for a long time (longer than 10 Myr) in the absence of sufficient compression, except for plates with very strong (especially lower crustal) rheology. Otherwise, the folds either will be flattened by gravity-driven crustal flow associated with the large crust–mantle density contrast at the Moho, or deformation will localize along some of the faults created at the inflection points of folds.

The fact that folding with wavelengths of 400–500 and 500–600 km persists long after cessation of the compression in the presumably high-rigidity Australian craton and Russian platform points to a strong rheology yielding a high value for the EET (in excess of 60 km), as expected from its thermo-mechanical age (Beekman *et al.*, 1997). The long wavelengths of 400–600 km of crust–mantle down-warping in the eastern Barents Sea, where Mid-Cenozoic compression has affected a basin system formed during Late Permian-Triassic time (Ritzmann & Faleide, 2009), with a total infill of sediments of the order of 15–20 km is another impressive example of compressional deformation on relatively cold lithosphere.

Most of the areas with present-day long-wavelength continental lithosphere folding formed during or shortly after the Alpine collision 60 Myr ago. It thus seems that 60 Ma is a characteristic timescale of gravity collapse of the large-scale folds in such intermediate-age lithospheres. In the case of very weak quartz-dominated lower crust, folds may disappear rapidly within 8–15 Myr. Experiments (Cloetingh *et al.*, 1999) for 1000-Ma-old lithosphere, with a diabase lower crust, demonstrate that folding-induced deformation persists for 10–50 Myr following the cessation of compression. During this period, the amplitude of the folds decreased by $<10\%$. At this stage, crustal faults may accelerate the gravity collapse of folds, creating inverted basins.

BASIN GEOMETRY AND ACCOMMODATION SPACE

Basin shape

Folding of the lithosphere leads to a symmetrical pattern of down-warped areas (synclines) flanked by highs (anticlines) of similar amplitude and wavelength, like for instance the Ferghana basin in Central Asia (Burov & Molnar, 1998).

This symmetry is in marked contrast to the asymmetrical shape of FBs, formed by flexure in front of an orogenic wedge, which are flanked by a flexural bulge of an amplitude that is only up to 10% of the maximum depth of the foreland depression (Royden, 1988; Zoetemeijer *et al.*, 1999). Both types of compressional basins show linear alignment of parallel depocentres and flanking highs. An important difference is the presence of parallel trending depocentres for lithospheric folding, whereas foreland flexural basins have a single depositional system. In addition, basins developed on folded lithosphere have a static location of the axis of their depocentres, in contrast to FBs, where the axis of depocentres can migrate with time (e.g. Zoetemeijer *et al.*, 1993).

In both cases, the integrated strength of the lithosphere (Watts & Burov, 2003; Tesauro *et al.*, 2007) defines the characteristic width of the basins. For folding, basin width roughly corresponds to one half of the fold wavelength (λ), which equals five to 10 times the thickness of the strong core of the lithospheric plate, h ($h = 10$–100 km, i.e. $\lambda = 50$–1000 km). In the case of crust–mantle decoupling, which occurs in relatively young plates, two dominant folding wavelengths develop (typically 250–400 and 50–100 km). Thus, two basin populations may be observed, one imbricated within the other. In the case of flexural foreland deformation, the width of the basin is controlled by the flexural parameter and is thus of the same order as the largest fold wavelength.

Subsidence patterns

Lithospheric folding results from instability in the lithosphere due to stress/strain incompatibilities that develop in rheologically stratified layers under compressive strain. This process typically operates with timescales of the order of 1–10 Myr (Cloetingh *et al.*, 1999). The preservation of lithospheric folds appears to depend strongly on the thermo-mechanical age of the underlying lithosphere (Cloetingh *et al.*, 1999). Folds in young lithosphere will not be preserved upon relaxation of the stress field, whereas ones in cratonic lithosphere will be well preserved (Cloetingh *et al.*, 1999).

Figure 11a displays characteristic basin subsidence patterns predicted by folding of 150 and 300-Ma-old lithosphere due to a 3 cm year^{-1} shortening rate. As illustrated (Fig. 11b), the differential motions occur in three distinct phases:

Stage 1 is the basin formation phase, coinciding with the initiation and development of folding, which is marked by an acceleration of subsidence in the basin and uplift in the flanking highs. As a result of the time lag between sediment supply and the creation of accommodation space, during the few Myr needed to form the basin, deposition cannot keep up with subsidence causing sediment-starved basins. A similar pattern occurs in PAB (Pitman & Golovchenko,

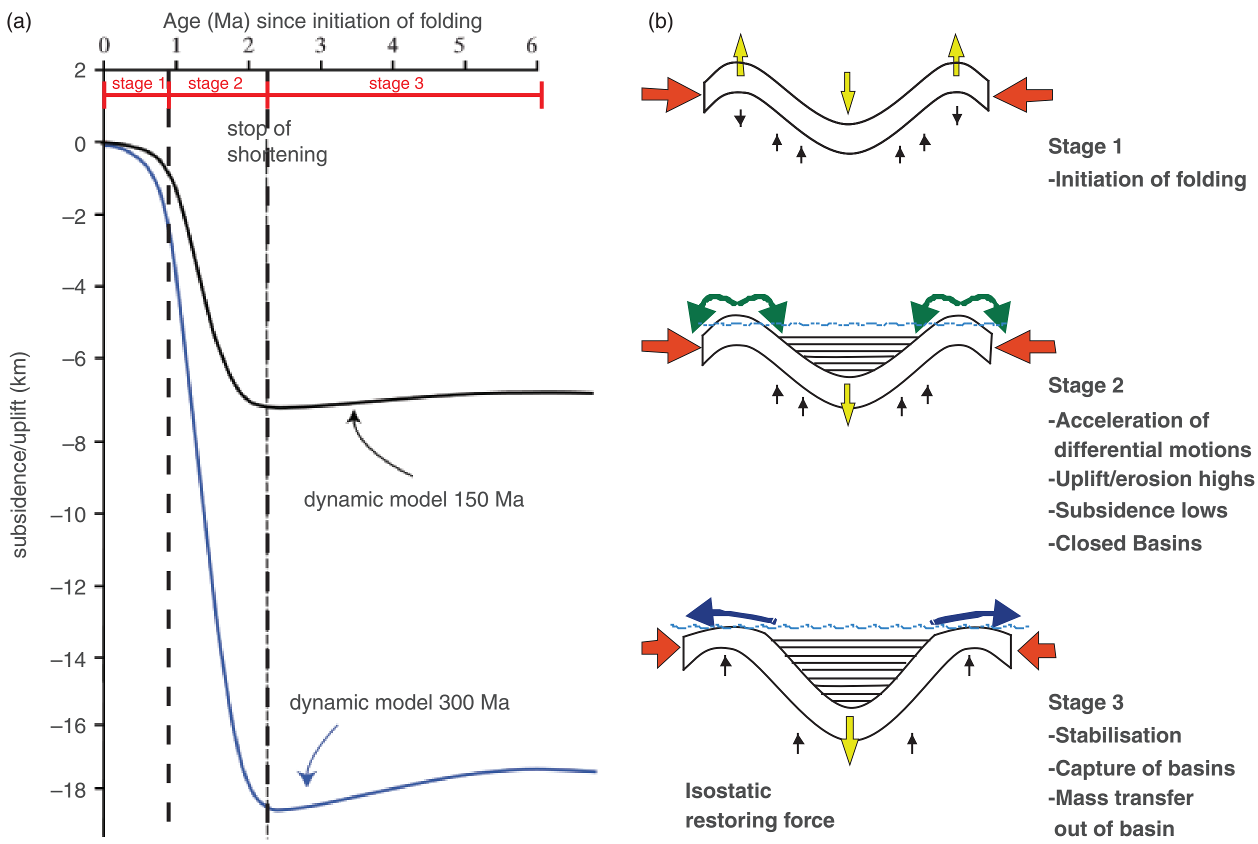

Fig. 11. (a) Characteristic subsidence patterns in centre of synclinal depression for thermo-mechanical age of 150 and 300 Ma, respectively. Shortening rate is 3 cm year^{-1}. (b) Characteristic stages in the evolution of a basin formed by lithospheric folding. Stage 1: Basin formation stage, acceleration of subsidence and uplift during folding. Stage 2: Steady-state: equilibrium between tectonic subsidence and sediment supply from eroding highs. Stage 3: Capture of folded basin; overall uplift and erosion. Wiggled waved blue line marks position of base level.

1983), which are also associated with ultra rapid subsidence in their formation stage also lasting only a few Myr.

Stage 2 is the basin preservation stage, where equilibrium develops between sediment supply and sediment deposition. As a result, the basin will be rapidly filled to overfilled.

Stage 3 is the basin destruction phase, characterized by basin capture and removal of sediments to areas outside the folding system. During this phase, the size of the accommodation space is reduced and erosion occurs on both flanks and depocentre. Thus, the net effect of these three stages is that lithospheric folding will lead to the development of distinct depositional–erosional cycles.

Characteristic patterns for vertical motions for folding of continental lithosphere of 150 and 300-Ma-old (Fig. 11) demonstrate a remarkably short time scale in which substantial amounts of tectonic subsidence are induced by the process of lithospheric folding. As shown by Fig. 11, within 1 Myr after the initiation of folding induced by shortening the lithosphere at a rate of 3 cm year^{-1}, subsidence rates are in the order of 5–15 km Myr^{-1}, depending on the thermo-mechanical age of the lithosphere. Thus, folding appears to be more effective in middle-aged lithosphere of 300 Ma than in lithosphere of younger ages (Cloetingh *et al.*, 1999; Burov & Cloetingh, 2009). After 2 Myr, a slow uplift phase starts of relatively minor magnitude of the order of a few hundreds of metres up to a kilometre. The predicted subsidence in Fig. 11 is for the centre of the syncline. As pointed out above, erosion of the uplifted flanks is taken into account, adopting a diffusive equation approach to erosion (see Burov & Cloetingh, 1997; Cloetingh *et al.*, 1999, for further details).

The alignment of parallel highs and basins of similar dimensions has an important consequence for the areal extent of the source areas for sediments available for deposition in the folded depressions. In comparison with FBs, the distribution of sources is more symmetrical, superseding the volume of sediments that can be eroded from, for example, the flexural foreland bulge. As noted earlier, erosion reduces the contribution of gravity-dependent terms and accelerates local deformation. Erosion, therefore, has an important feedback with the geometry of the accommodation space in changing the spectrum of wavelengths (Cloetingh *et al.*, 1999). Erosion acts as a filter, suppressing the shorter wavelengths in folded basin topography. Strong erosion, insufficiently compensated by tectonic deformation, can even wipe out most of the topography. However, if the erosion is tuned to the average elevation rates (Fig. 12), it may dramatically accelerate folding (Cloetingh *et al.*, 1999).

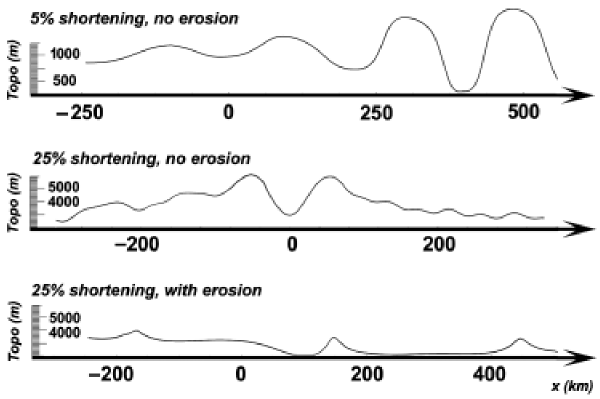

Fig. 12. Illustration of the effect of erosion, which acts as a filter suppressing the short wavelengths. In this case, the wavelength and amplitude vary along the cross section at different stages of deformation due to a partial crust–mantle coupling and strain localization for a 400 Ma old lithosphere with weak quartz-dominated rheology. After 5% shortening (top), after 25% shortening (middle), after 25% shortening (bottom), strong zero order diffusional erosion (Avouac & Burov, 1996) tuned to keep mean elevation at the level of 3000 m. Erosion reduces the contribution of gravity-dependent terms (middle wavelength) and accelerates local deformation. Strong erosion, insufficiently compensated by the tectonic deformation wipes out most of the topography (after Cloetingh *et al.*, 1999).

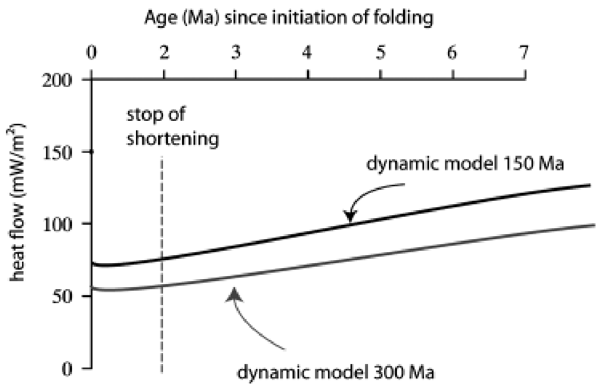

Fig. 13. Thermal consequences of lithosphere folding, and associated basin evolution depicted in Fig. 11. The heat flow response is marked by an initial decrease in heat flow as a consequence of rapid sedimentation, followed by a progressive long-term heat flow increase after termination of shortening. Thermal conductivity of sediments is 2.5 W m^{-1} C^{-1}. Surface radiogenic heat production H_s is 9.5×10^{-10} W kg^{-1}. Concentration of radiogenic heat sources within sedimentary basin fill is homogeneous. Exponential decay of heat production is assumed for underlying crustal rocks. Note that the figure shows only 7 Ma of thermal evolution. The heat flow does not increase anymore after some tens of Ma and subsequently decreases at later stages.

There has been a rapid development and application of stratigraphic modelling packages to sequence stratigraphy over the last two decades (e.g. Cross, 1989; Alzaga-Ruiz *et al.*, 2008). Among the different types of modelling programs, the forward stratigraphic modelling approach has been applied extensively by basin modellers from academia and petroleum industry (e.g. Lawrence *et al.*, 1990; Granjeon, 2009). Forward stratigraphic modelling commonly starts with an estimate of the initial conditions related to an adopted basin formation mechanism and controlling parameters, followed by a forward prediction in time. Most of these software packages are based on sequence stratigraphic concepts (Wilgus *et al.*, 1988). Assumptions for initial subsidence are either ad-hoc or related to stretching (e.g. Lawrence *et al.*, 1990) or foreland flexure (Garcia-Castellanos *et al.*, 1997), but to date do not include lithospheric folding as a basin formation mechanism.

Marine vs. continental deposits and closed basins vs. capture of drainage

Erosion of uplifted areas and sedimentation in the depressions created by folded lithosphere is a self-reinforcing process promoting continuing uplift of the highs and subsidence in the depocentres. Thus, such basins will remain closed during much of their evolution. Folded basins will hence be predominantly characterized by continental deposits with only minor deposition of marine sediments during marine incursions or during basin capture. This seems to be the case for folded basins in Iberia (e.g. Duero Basin) and Central Asia (Ferghana, Tarim Basin, Lake Issyk-Kul) (Cobbold *et al.*, 1993). As has been pointed out for flexural FBs (Garcia-Castellanos *et al.*, 2003), the capture time for opening basins decreases with an increasing flexural rigidity. The flexural upwarp to restoring the topography removed by erosion will be almost instantaneous for very weak lithosphere, but requires up to 50–100 Myr for high lithospheric rigidities (Garcia-Castellanos *et al.*, 2003). Thus, basins created by folding of cratonic lithosphere probably have a shorter capture time than ones formed in younger lithosphere.

THERMAL REGIME, STRESS REGIME AND STYLE OF FAULTING

Thermal regime

Lithospheric folding is controlled by the interplay of lithospheric stresses and inherited strength of the lithosphere. The thermal regime controls the rheological profile and differs between folded basins developed in young lithosphere and basins in cratonic lithosphere. The latter are associated with much lower thermal gradients than basins developed on young continental lithosphere. As for FBs, the initiation of folding is not associated with a thermal instability, unless folding occurs in conjunction with plume activity (Burov & Cloetingh, 2009). Following the deposition of radiogenic sediments in the folded depression, sediment blanketing will affect the heat flow (Stephenson *et al.*, 1990; Lavier & Steckler, 1997; Van Wees *et al.*, 2009), modifying the surface heat flow in the basin centre. As pointed out by Lavier & Steckler (1997) and

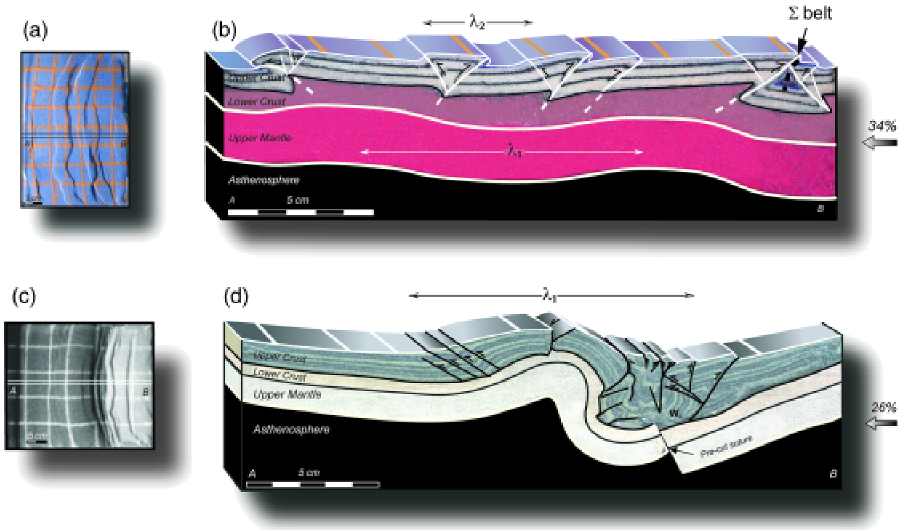

Fig. 14. Results of analogue tectonic experiments for lithospheric folding (after Sokoutis *et al.*, 2005) (Top): folding of uniform lithosphere. Cross section demonstrating pop-up structures in the upper crust above highs induced by lithospheric folding. λ_1 and λ_2 indicate first-order and second-order wavelengths, respectively. Imbrication of bivergent thrust wedges is responsible for the relatively high topography belt (Σ-belt) at the right-hand side of the model and closure of prismatic basins with a rather undisturbed bottom. The progressive sinking of the prismatic basin allows transferring of the crustal material (i.e. cover sediments) that was initially situated at the surface of the model down to significant depth. Left-hand side (a) final top view of model after 34% of bulk shortening. Right-hand side (b) cross section located on the top view. Arrows indicate the direction of the moving wall. Note the similarity to Central Iberia (Fig. 5). (Bottom): Geometries predicted by analogue experiment, shortening a lithosphere with two contrasting blocks, bounded by suture. A deep synclinal depocentre develops over the suture zone, flanked by an anticline of smaller amplitude. Left-hand side (c) final top view of model after 26% of bulk shortening. Right-hand side (d) cross section located on the top view. λ_1 indicates a first-order wavelength of the folding. Note the striking similarity to the configuration of the South Caspian Basin/Alborz Mountain system displayed in Fig. 8.

Ziegler *et al.* (1998), the effect of sediment fill is to weaken the lithosphere. The low thermal conductivities of the sediments lead to high temperatures in the upper lithosphere and consequently low local yield strength. During basin subsidence, sediments deposited in the central parts of the basin might be exposed to temperature windows corresponding to hydrocarbon generation. At the same time, sediments pre-dating the folding may have undergone extra burial due to syn-folding sedimentation. An example is the Paris basin, where source rocks of Toarcian age were folded in Cenozoic time (Guillocheau et al., 2000; Le Solleuz *et al.*, 2004).

During basin capture, overall cooling occurs. This effect is illustrated by characteristic thermal evolution for different thermo-tectonic ages of 150 and 300 Ma of the folded continental lithosphere, incorporating radioactive heat production in the sediments filling in the synclinal depression, shown in Fig. 13. Subsidence induced by folding is calculated for the centre of the basin. Basins developing on folded lithosphere are characterized by their relatively low heat flow at the onset of folding, followed by a steady increase with time, doubling the heat flow over a time interval of the order of 5 Myr following the cessation of shortening. This increase is primarily due to the contribution of radioactive heat production in the very substantial pile of sediments accumulating in a relatively short time interval. The patterns of heat flow are similar for different thermo-mechanical ages of the lithosphere, with the oldest lithosphere having the lower heat flow. Older ages enhance the accommodation space and the contribution of the sediments to heat flow but are compensated by a larger decrease in heat flow with ageing lithosphere. Another important factor is the mode of folding. Crustal scale folding, which is characteristic for Lake Issyk-Kul, will be associated with shorter wavelengths, shallower basin depths and thinner sequences of heat-producing sediments than for mantle lithospheric folding. This effect might explain the relatively low heat flow observed in Lake Issyk-Kul (Vermeesch *et al.*, 2004).

Modes of brittle deformation and faulting

The role of pre-existing faults on the development of folding has been investigated through numerical experiments on folding of brittle-elasto-viscous lithosphere (Beekman *et al.*, 1996; Gerbault *et al.*, 1998; Cloetingh *et al.*, 1999) and through analogue experiments on plastic–elastic lithosphere (e.g. Martinod & Davy, 1994; Sokoutis *et al.*, 2005). These studies show that lithospheric folding and faulting can develop simultaneously and that pre-existing crustal scale faults do not prevent, but instead promote the development of folding instabilities. The instabilities, in turn, can initiate the formation of new faults at the inflection points of the folds. Although the usual expectation is that faulting prevents folding, this view neglects the role of the gravity and friction on faults in the behaviour of the large-scale fault-and-fold systems. As also observed in analogue experiments (Martinod & Davy, 1994), this continuous behaviour of faulted lithosphere can be explained by fault locking due to gravity and friction. After some sliding (uplift) on a fault, the potential gravitational energy working against friction generated by horizontal shortening forces becomes too high. As a result, the fault locks and the rock mass transmit horizontal stresses as a continuous medium. As the compression continues, one of the folds finally starts to grow faster than others, resulting in a loss of the periodicity and the formation of a mega-fold (see also the discussion in the context of the Ferghana and Tadjik basins of Central Asia).

Following the initiation of folding, and the further build up of compressional stresses, folding will, therefore, usually be accompanied by brittle deformation and faulting in the crust and upper lithosphere. The surface expression of folding in uniform lithosphere is frequently in the form of fault-controlled pop-up and pop-down structures and inverted basins (e.g. Cobbold *et al.*, 1993), accompanied by the development of imbrications of bivergent thrust wedges at the areas where shortening is applied (Sokoutis *et al.*, 2005). These findings (see Fig. 14) are corroborated by observations in the Central System of Iberia, where folding of Variscan lithosphere with a thermo-mechanical age of 280 Ma occurs (Cloetingh *et al.*, 2002). Here, the brittle deformation associated with crustal scale folding expressed by a folded Moho is mechanically decoupled from folding of the mantle lithosphere (Fernandez-Lozano *et al.*, 2010; see Fig. 5b).

Crustal and mantle faults may develop as a result of folding (Burov & Molnar, 1998) (Fig. 15). Folding can continue after these faults develop and folding and faulting can co-exist for times of several Myr (Fig. 5b). For crust–mantle decoupling, a complex distribution of crustal faults and surface undulations can be expected, with crustal faults not necessarily connected to mantle faults. Numerical experiments suggest that mantle faults are unlikely to be longer than a few km in depth (Burov & Molnar, 1998). Such faults may also not develop at longer wavelengths of folding connected with stronger lithosphere. However, deep-seated faults in mantle lithosphere can develop when cratonic lithosphere is folded (Cloetingh *et al.*, 1999). The mode of faulting, depth extent and spacing of faults depend on the thermo-mechanical age of the lithosphere. Once the development of folding begins in a basin, the intensity and depth penetration of faulting will accelerate. The mode of decoupling between crustal and mantle folding is crucial. Discontinuities within the folded lithosphere will localize the development of deep synclines, flanked by more modest anticlines (Sokoutis *et al.*, 2005) and affect the distribution of faulting (Fig. 14).

During the next phase of basin evolution, when a steady state is reached between the creation of accommodation space and sediment supply, only minor faulting will occur. This is in marked contrast with the later phase of basin capture, which is in general characterized by erosion and narrowing of the basin. Owing to erosional unloading, stress relaxation will occur, manifested in upward propagating faults.

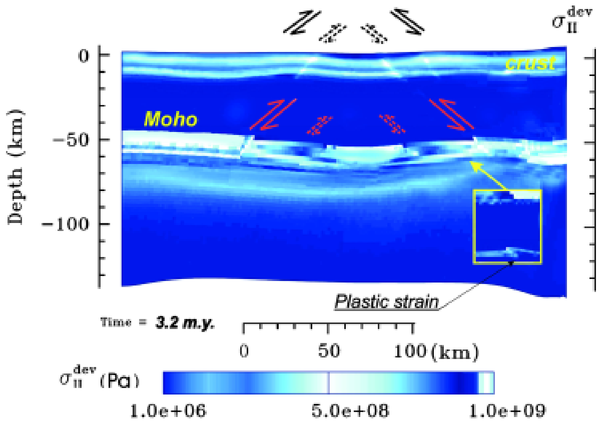

Fig. 15. Numerical experiment on faulting developed in folded continental lithosphere of 150 Ma (Burov & Molnar, 1998). Note different wavelengths of the crustal and mantle part of the lithosphere and differences in spacing and character of faults that are conditioned by folding. In each layer, two fault spacings occur: a shorter one proportional to layer thickness (also controlled by the strength contrast between the stiff layer and embeddings), and the longer wavelength controlled by the wavelength of folding. The inset shows plastic (brittle) strain localization characterizing initialization of mantle faulting.

Interaction of folding with other tectonic processes

Folding, in addition to being a basin-forming mechanism, frequently interacts with other tectonic processes. As pointed out by Cloetingh (1988), intraplate compression can modify pre-existing basins. As discussed above, the Pannonian Basin of Central Europe created by Miocene back-arc extension appears to be an example of such a configuration, characterized by atypical aperiodic folding. Other examples are cratonic sag basins where intraplate compression (Cloetingh, 1988) is thought to occur in interaction with phase changes in the lithosphere (Artyushkov, 2007). Examples of these might be the Barents Sea (Ritzmann & Faleide, 2009) and possibly the South Caspian Basin, although in the latter case pre-orogenic extension cannot be ruled out (Guest *et al.*, 2007). Basins exposed to changes in tectonic regime will have a polyphase record (Cloetingh & Ziegler, 2007), characterized by a superposition of more than two regimes, such as pre-orogenic extension, foreland flexure and late-stage folding. This sequence appears to be characteristic for some very deep FBs, such as the Focsani depression of the Romanian Carpathians, with more than 16 km of sediments, which was affected by extension due to the opening of the Black Sea Basin, followed by foreland flexure and overprinted by Late Miocene compression (Tarapoanca *et al.*, 2003). As pointed out above (Ziegler & Dèzes, 2007), the Northwestern European foreland indicates folding, which overprints the rifting and foreland flexure. Quantification of the topographies created by rifting and foreland flexure and correcting for them is essential to reconstruct the shape of the additional accommodation shape created by subsequent lithospheric folding (Bourgeois *et al.*, 2007).

The impingement of plumes on the base of continental lithosphere can induce differential topography similar to the surface deflections characteristic for lithosphere folds (Burov *et al.*, 2007; Guillou-Frottier *et al.*, 2007). Plumes and lithospheric folds frequently interact in space and time in the geological record (Ziegler & Dèzes, 2007; Burov & Cloetingh, 2009). Therefore, the evolution of FLBs can be overprinted by the signatures of a plume or vice-versa. This will lead to an amplification of the induced vertical motions, particularly significant for young and intermediate age lithosphere. Emplacement of hot upper mantle material will raise temperatures in the lithosphere and increase heat flow. Owing to the lag time in the propagation of heat, the effect at the surface might become manifest only after several tens of Myr. Plume emplacement might also weaken the lithosphere, making it more prone to compressional fault reactivation after cessation of the folding.

Interplay of lithosphere folding and plume impingement on the continental lithosphere occurred probably almost simultaneously in late Neogene times in the Northwestern European foreland. Two examples are the Eifel and Massif Central areas of the Alpine foreland of NW Europe (Cloetingh & van Wees, 2005; Ziegler & Dèzes, 2007). Both areas are sites of main Late Neogene volcanic activity in the ECRIS. Seismic tomography (Ritter *et al.*, 2001) shows finger-shaped baby plumes with a characteristic spatial diameter of 100 km, extending downward to 400 km. Ziegler & Dèzes (2007) propose that plume activity occurs simultaneously with recent compressional deformation in the Massif Central area (Guillou-Frottier *et al.*, 2007) and the Ardennes/Eifel area. Geomorphological studies constrain the recent uplift of the Ardennes and the Eifel area. An order in magnitude difference occurs between the uplift of the Eifel area, underlain by a plume and the adjacent Ardennes area where evidence for a plume is lacking. The patterns of uplift appear to be radial, superimposed by a linear NE–SW trend perpendicular to the main axis of compression. Baby plumes primarily develop in the anticlines of lithospheric folds (Burov & Cloetingh, 2009). The plume activity presumably accelerated the rate of uplift by a factor of 3–5 (Cloetingh & Ziegler, 2007). According to presently available data, the plumes in this segment of the ECRIS arrived about 1 Myr ago. This activity was preceded and followed by lithospheric folding that continues to the present day since 17 Myr ago (Bourgeois *et al.*, 2007).

Thermo-mechanical modelling illustrates the relative effectiveness of amplification of lithosphere deformation and topographic effects induced by plumes through folding and vice-versa. Burov & Cloetingh (2009) examined the response times and time-lags involved and whether these baby plumes were more efficient in localizing deformation than large plumes. Plume-affected folding appears to accelerate surface uplift, whereas folding goes into saturation and stagnates when plastic hinges form. For the discrimination of plumes and folding, it is critical to access constraints on the presence or absence of radial vs. linear symmetry, heat flow anomalies, gravity and geoid data. Plume activity facilitates folding, by dramatically lowering the stress levels required (Burov & Cloetingh, 2009). Plume impact also reduces the fold wavelength and localizes folding above the plume impact area. A general outcome of the modelling and observations is that lithospheric folding as a mechanism for producing thermal perturbations in the lithosphere/upper mantle system is a less feasible scenario.

FOLDING AND OTHER MODES OF BASIN FORMATION: DIFFERENCES AND SIMILARITIES IN STRUCTURE AND EVOLUTION

Sedimentary basins formed through lithospheric folding have characteristic features including vertical motions, basin architecture, thermal regime and fault activity, distinguishing them from other basin types (Cloetingh & Ziegler, 2007; Xie & Heller, 2009). Figure 1b and Table 2 illustrate differences and similarities between basins developed on FLB, FB, ICB, EB and PAB.

Sedimentary basin systems are, by their nature, prone to tectonic reactivation, and therefore, frequently characterized by a poly-phase evolution (Cloetingh & Ziegler, 2007). EB are, for example, often formed in areas thickened previously by tectonic compression and subsequently often subject to late-stage compression (Lundin & Doré, 1997). Examples include the Pannonian basin of Hungary (Horváth & Cloetingh, 1996) and the North Atlantic rifted margins (Cloetingh *et al.*, 2008). Similarily, FB are frequently characterized by pre-orogenic extension. Examples include the Carpathian foredeep (e.g. Tarapoanca *et al.*, 2003) and the Aquitaine basin of Southern France, which was the retro-arc FB of the Pyrenees (Desegaulx *et al.*, 1991). The actual subsidence patterns of these polyphase systems are often more complex than predicted by the end-member models discussed below that only consider the basin formation mechanism. Retro-arc FBs are characterized by a prolonged subsidence history with a distinct thermal signature including the effects of thermal cooling inherited from pre-orogenic extension. This is sometimes neglected in comparing pro-arc and retro-arc FBs (Naylor & Sinclair, 2007).

Basin infill records allow main features, including geometry, vertical motions and faulting characteristics to be unravelled (Zoetemeijer *et al.*, 1993). However, heat flow histories need to be determined through kinematic reconstruction and forward modelling. Results of heat flow history modelling for FB and EB settings (Van Wees *et al.*, 2009) can be subsequently compared with FLB results presented in this paper (Fig. 13). For ICB and PAB, we have refrained from a quantitative approach for heat flow predictions as vertical motions driving subsidence cannot be linked in a straightforward way to a single or uniformly distributed lithosphere process. As a consequence, for these settings tentative heat flow patterns have been drawn.

Table 2. Key characteristic features of different classes of sedimentary basins

Basin type	Basin shape	Dimensions	Subsidence characteristics	Thermal evolution	Faulting history
FLB	Symmetrical	Width: 50–600 km; depth: up to 20 km	Accelerated subsidence, time scales 1–10 Myr; simultaneously uplift at highs	No initial heating; heat flow increases in first 10 Myr with sediment deposition and burial, and subsequently decreases	Intensive deformation, accelerating trough basin formation phase
FB	Asymmetrical	Width: 50–250 km; depth: up to 10 km	Linear subsidence, interrupted by short-lived faster subsidence during thrusting phases; timescales 10–100 Myr; simultaneously uplift from thrust front and foreland bulge	No initial heating; heat flow increases with time with sediment deposition and burial	Faulting and thrusting limited to orogenic wedge; minor deformation through faulting in foreland
EB	Symmetrical (pure shear); asymmetrical (simple shear)	Width: 30–500 km; depth: up to 10 km	Rapid initial subsidence, followed by post-rift decay in subsidence; in case of multiple rifting repeated accelerated subsidence; time scales for post-rift subsidence of the order of 70 Myr; At rifting stage development takes place of asymmetrical rift shoulder topography, flanking the rift	Initial heating event, followed by decaying heat flow	Extensional faulting limited to basin formation phase; during post-rift absence of faulting
PAB	Symmetrical	Width: 20–50 km; depth: up to 10 km	Very rapid initial subsidence, followed by post-rift decay in subsidence, time scales: 1–10 Myr in early stage, sedimentation cannot keep up with subsidence	Initial heating event, followed by very rapid decay in heat flow	Extensional faulting limited to basin formation phase; during post-rift absence of faulting
ICB	Symmetrical	Width: 500–1000 km; depth: up to 10 km	Slow subsidence, punctuated by periods of faster subsidence, possibly related to large-scale tectonic events; Characteristic time scales: 500–800 Myr	In absence of understanding of basin formation mechanism no prediction for initial heat flow; heat flow at later stage dominated by burial history	Very low level of faulting throughout tectonic history

FLB that develop as a result of periodic folding are highly symmetrical, with dimensions that can vary from 50 to 600 km, depending on lithospheric age and shortening rate. These basins can accumulate thick sedimentary sequences up to the order of 20 km. The time scales associated with this process of basin formation are very short, typically a few Myr. The subsidence is so fast that erosion and sediment supply at the basin formation stage typically lag behind, leading to the development of starved basins, followed by shallowing upward sequences after stress relaxation. Subsidence patterns are characteristically convex upwards with time. A noticeable feature is the development of significant topography of the order of several km flanking the synclinal depression. No initial heating is predicted, with an increase in heat flow with time following the basin formation. Significant brittle deformation is expected to occur in the folded basement, accelerating during the folding phase.

FB are strongly asymmetrical, with depths usually < 10 km, and have modest flexural bulges of a few hundred metres (Royden, 1993; DeCelles & Giles, 1996; Zoetemeijer *et al.*, 1999). Important differences occur in the nature of the subsidence of pro- and retro-FB (Naylor & Sinclair, 2007). The first are typically associated with short life spans and convex up subsidence patterns with time, whereas the latter show more prolonged subsidence histories and concave up subsidence patterns. Subsidence patterns will be interrupted during thrusting phases, also leading to uplift of the flexural marginal bulge (Quinlan & Beaumont, 1984; Zoetemeijer *et al.*, 1993). The predicted heat flow pattern of a pro-foreland setting shown for the Ebro FB (well Jabali from Verges, 1999), marked by rapid basement subsidence and sedimentary infill of *ca*. 4 km in *ca*. 10-Myr period (other parameters as in Van Wees *et al.*, 2009). Flexure and rapid sediment infill is marked by a reduction of heat flow, followed by a progressive increase related to radiogenic heat production of foreland sediments. Basement fracturing is concentrated at the points of maximum curvature in the flexed lithosphere, at the maximum points of upward and downward deflection, respectively, with intensity higher than inferred for FLB.

ICB share their symmetrical shape and great thickness of their sedimentary basin fill with FLB. An important difference is their evolution in time, characteristically associated with very long time spans (typically of the order of 500–800 Myr) with long phases of low subsidence rate punctuated by phases of subsidence acceleration. As pointed out above, this is why ICB are probably affected by short-term phases of enhanced intraplate compression superimposed on other mechanisms operating on longer time scales. The large dimensions of these basins point to formation in high-rigidity lithosphere that freezes in basin deformation over long time scales. The long time scales involved also imply that the highs induced by compressional upwarping will be commonly eroded. A major difference between ICB and FLB is that current hypotheses for ICB formation are cast only in terms of the tectonic processes operation at their earlier stage such as phase changes in the lithosphere. It appears, therefore, that lithospheric stress fields and the lithosphere rheology (inferred from gravity and flexure) are far more diagnostic than the lithosphere–asthenosphere boundary, which is only giving information on the thermal state of the lithosphere. Heat flow patterns of ICB will be dominated by sediment infill. ICB are in general characterized by a low intensity of faulting. However, in the absence of a rigorous understanding of the formation mechanisms of ICB, predictions for heat flow are often not available. As a consequence, their heat flow is most often described primarily in terms of the thermal consequences of their burial history.

EB have received major attention from basin modellers, both because of their relative abundance and importance and because of the availability of a relatively simple quantitative model for their formation (McKenzie, 1978). The latter can be relatively easily incorporated in forward

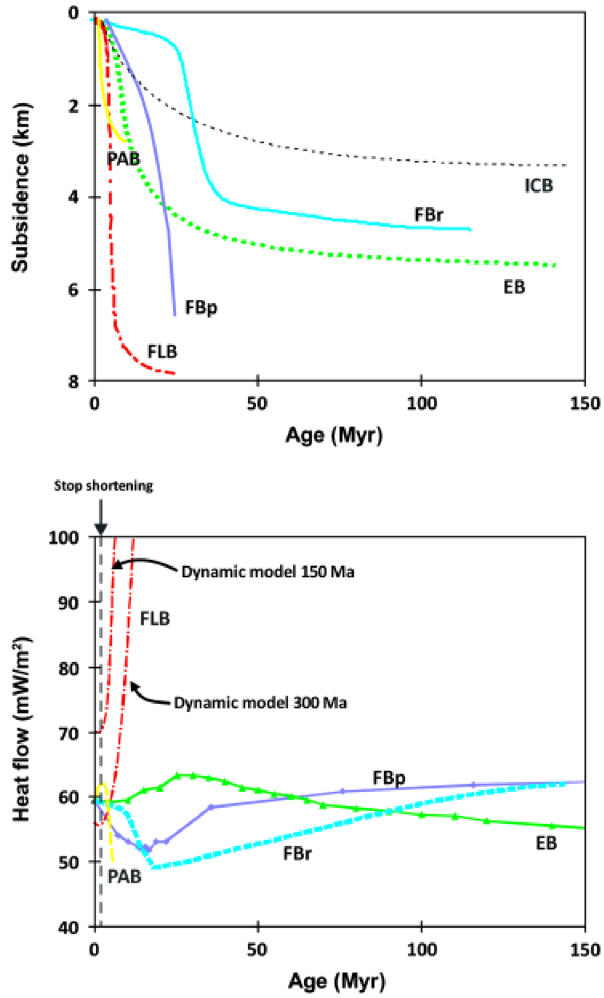

Fig. 16. Comparison of main characteristics of basins developed on folded lithosphere (FLB with a shortening rate of 3 cm year^{-1}) with other basin types, including foreland basins (FBr, retro-arc foreland basin; FBp, pro-arc foreland basin), intracratonic basins (ICB), extensional basins (EB) and pull-apart basins (PAB). Different panels give theoretical predictions. Top: Basin subsidence history in basin centre. Bottom: Thermal history. See text for explanation.

Table A1. Notations and physical values common for all experiments (Schubert *et al.*, 2001; [150]Turcotte & Schubert, 2002)

Parameter	Values and units	Definition
σ, τ	Pa, MPa	Stress (complete, deviatoric)
P	Pa, MPa	Pressure
u	m, mm	Displacement vector
v	$m\,s^{-1}$, $mm\,an^{-1}$	Velocity vector
$\dot{\varepsilon}$	s^{-1}	Strain rate
μ	10^{19}–10^{25} Pa s	Effective viscosity ($\tau/\dot{\varepsilon}$)
T	°C, K	Temperature
h_c	40 km	Moho depth
h_l	100–250 km	Thickness of lithosphere
D	100–200 km	Plume diameter
ρ_l	3330 kg m^{-3}	Density of mantle lithosphere
ρ_m	3340 kg m^{-3}	Reference deep mantle density
ρ_p	$\rho_m+\Delta\rho_{ch}+\alpha\rho_m\Delta T$	Plume density
$\Delta\rho_{ch}$	0–25 kg m^{-3}	Chemical density contrast
g	9.8 m s^{-2}	Acceleration due to gravity
C_p	10^3 J Kg^{-1} °C^{-1}	Specific heat
ΔT	250 °C	Initial temperature contrast plume – background
α	3×10^{-5} °C^{-1}	Thermal expansion coefficient at 0 km depth
β	8×10^{-12} Pa^{-1}	Isothermal compressibility

Table A2. Specific rheology and related thermal parameters

Parameter	Value
All rocks	
λ, G Lamé elastic constants ($\lambda = G$)	30 GPa (above 250 km depth)
λ, G Lamé elastic constants ($\lambda = G$)	60 GPa (below 250 km depth)
ϕ friction angle (Mohr–Coulomb criterion)	30°
C_0 cohesion (Mohr–Coulomb criterion)	20 MPa
Specific upper or weak (quartz) lower-crust properties	
ρ (upper crust)	2700 kg m^{-3}
ρ (lower crust)	2900 kg m^{-3}
n	2.4
A	6.7×10^{-6} MPa^{-n} s^{-1}
Q	1.56×10^5 kJ mol^{-1}
Specific strong lower crust properties (diabase or basalt)	
ρ	2980 kg m^{-3}
n	3.4
A	2×10^{-4} MPa^{-n} s^{-1}
Q	2.6×10^5 kJ mol^{-1}
Specific mantle properties (olivine)	
ρ (lithosphere)	3330 kg m^{-3}
n	3
A	1×10^4 MPa^{-n} s^{-1}
Q	5.2×10^5 kJ mol^{-1}
Thermal model	
Surface temperature (0 km depth)	0 °C
Temperature at the bottom of thermal lithosphere	1330 °C
Temperature at 660 km depth	2000 °C
Thermal conductivity of crust k	2.5 W m^{-1} °C^{-1}
Thermal conductivity of mantle k	3.5 W m^{-1} °C^{-1}
Thermal diffusivity of mantle χ	10^{-6} m^2 s^{-1}
Surface radiogenic heat production H_s	9.5×10^{-10} W kg^{-1}
Radiogenic heat production decay depth h_r	10 km
Thermo-tectonic age of the lithosphere a	60 (young) to 1000 Ma (old)

Compilation by Burov *et al.* (2001). ρ is density; Q, n, A are material-dependent parameters of ductile flow laws (Kirby & Kronenberg, 1987; Kohlstedt *et al.*, 1995). Other parameters from Turcotte & Schubert (2002).

modelling of their subsidence and heat flow histories (Van Wees *et al.*, 2009). The basin shape is symmetrical or asymmetrical depending on a pure shear or simple shear mode of extension. Rifts can be narrow or wide, depending on the mode of rifting and the rheology of the extending lithosphere (Huismans and Beaumont, 2002). Dependent on the rigidity of the extending lithosphere, rift shoulders with asymmetrical shape can be formed and be prone to erosion (Van Balen *et al.*, 1995; Van der Beek *et al.*, 1995). The development of rift shoulders and their erosion can lead to feedback with lower crustal flow and faulting in the extending lithosphere (Burov & Cloetingh, 1997). During the post-rift phase, flexural widening of the basin commonly occurs. A characteristic feature of EB predicted by simple stretching models (McKenzie, 1978) is the succession of rapid initial subsidence in the syn-rift phase and exponentially decaying subsidence in their post-rift phase with a typical thermally controlled time constants of the order of 70 Myr. Feedbacks between rift shoulder erosion and lower crustal flow (Burov & Cloetingh, 1997; Burov & Poliakov, 2001) have pronounced effects on subsidence in the final phases of rifting and in the early post-rift phase. Both can be influenced by changes in the mechanical properties of the lithosphere and its strengthening upon rifting. Multiple rifting phases are another common feature of EB. The duration of the syn-rift phase can vary from quasi-instantaneous (shorter than 20 Myr) to several hundreds of Myr (Cloetingh and Ziegler, 2007). In the latter case, basin migration is a common feature (Corti *et al.*, 2003). Extensional faulting occurs during the rift phase, with absence of faulting in the post-rift phase. Heat flow reaches a peak during the syn-rift phase, followed by a rapid decrease in heat flow (Van Wees *et al.*, 2009). The syn-rift peak in heat flow is low or almost absent in continental extensional settings as a consequence of removal of heat-producing elements in the crust and cooling by sediment infill. Figure 16 shows such a setting, which is based on the benchmark model presented in Van Wees *et al.* (2009), As a consequence of the loss of radiogenic heat production in the crust at the end of the post-rift stage values, heat flow evolves to values considerably lower than the initial ones. The EB heat flow pattern is, therefore, the reverse of that in FB where syntectonic heat flow is first lowered due to sediment infilling (Kombrink *et al.*, 2008), but eventually increases due to thermal relaxation and additional radiogenic heat production in the sediments.

PAB are characterized by a narrow fault bounded geometry (Smit *et al.*, 2008), developing over a very short time span. Models have been developed to calculate subsidence histories and heat flow histories for these basins (Pitman & Golovchenko, 1983), incorporating lateral heat transport in stretching models. These models predict rapid subsidence of several km's over time intervals of the order of 0.1–1 Myr, followed by a decay in the subsidence with a concave shape upward. Erosion and sediment flux cannot keep pace with the subsidence at the basin formation phase, leading initially to a starved basin, followed by a shallowing upward sequence (Pitman & Golovchenko, 1983). These basins are intensively faulted, also due to their strike-slip origin, whereas heat flow decays on very short time scales of the order of a few Myr. Although this scenario is a good first-order description, many PAB show a more punctuated fault controlled subsidence history, often terminating by late-stage uplift, as observed for Late Neogene PAB in the internal zone of the Betics in SE Spain (Cloetingh *et al.*, 1992) and for the flanks of PAB in the Dead Sea Fault System (Smit *et al.*, 2008, 2010).

From the above overview, it is apparent that FLB have in common with FB a compressional origin and thermal histories controlled to a large extent by burial histories. At the same time, pronounced differences occur in the duration of subsidence, varying from ultra short (FLB, one to tens of Myr), medium (FB, tens of Myr) and ultra long (ICB, hundreds of Myr). An important difference occurs in the spatial scales of the topography generated by folding and foreland fold-and-thrust belt deformation. In the latter case, a much steeper differential topography is generated over typical horizontal differences of the order of 10 km between peak and trough. In contrast, in the case of lithospheric folding horizontal distances between the topographic highs and the axes of the depocentres are typically of the order of hundreds of kilometres. As a result, diffusive transfer of mass will occur at a much slower rate of sediment supply in the case of folded lithosphere than rates of sediment supply locally generated by thrusting. This together with a very rapid initial subsidence of FLBs has important consequences for the palaeobathymetry of these systems.

FLB contrast with extensional and PAB in the shape of the subsidence curves, being convex up for FLB and concave for EB and PAB. The heat flow histories also differ. EB and PAB are characterized by a phase of initial heating, whereas FLB and FB are characterized by an absence of initial heating. A common feature of FLB and PAB formation is their capability to cause dramatic differential vertical motions in a short time interval, predicting shallowing upward sequences. FLB are to some extent unique in terms of the magnitude of the uplifted topography surrounding the down-warped depocentres. Similar magnitudes are only reached at rift shoulders of basins developing in intracratonic lithosphere (Van der Beek *et al.*, 1995). FLB can be associated with localized brittle deformation and pop-up structures in the upper crust and widespread brittle deformation at deeper crustal and upper mantle levels.

CONCLUSIONS

Sedimentary basins controlled by lithospheric folding are characterized by a number of features in their basin architecture, subsidence history, thermal evolution and faulting patterns making them distinctly different from other basin systems. Of particular importance are the relatively short temporal scales involved in their formation, whereas their spatial scales vary from tens to several hundreds of km, depending on the rheological stratification of the lithosphere and its thermo-mechanical age. Subsidence patterns are characterized by an acceleration of subsidence in the depocentres during compressional basin formation, occurring simultaneously with accelerated uplift of and erosion from flanking basin highs. In contrast with asymmetrical FB, basins on folded lithosphere are symmetrical with equal dimensions for linearly trending topographic highs and lows.

Basins on folded lithosphere have a strong tendency to remain closed systems during a major part of their evolution, with capture times decreasing with thermo-mechanical age from several tens of Myr to <10 Myr. The thermal history of these basins is not characterized by an initial thermal perturbation, unless folding occurs in interaction with plume activity. In the absence of an interplay with lithospheric-scale thermal perturbations, their thermal evolution will be primarily controlled by the burial history of the sediments deposited in the accommodation space created by the folding process.

Intrabasinal faulting and the formation of pop-up structures and inverted basins at upper crustal levels are important in the structural evolution of these basin systems. The intensity of the brittle deformation peaks with ongoing shortening of the lithosphere during folding but faulting activity is dramatically reduced after the cessation of folding. At this stage, with equilibrium between sedimentation and erosion, minor faulting occurs as a result of stress relaxation due to erosion of folded highs. During capture and overall uplift of basins on folded lithosphere, their accommodation space is further reduced by unflexing and associated stress release through faulting.

ACKNOWLEDGEMENTS

This work was initiated during S. Cloetingh's visit to Paris VI as a Visiting Professor and finalized during a subsequent Visiting Professorship at IFP. Comments and stimulating suggestions by Fred Beekman, Jan-Diederik van Wees, Francois Roure, Seth Stein, Jeroen Smit and Didier Granjeon are gratefully acknowledged. Thomas Kruijer and Elishevah van Kooten provided valuable technical assistance. We benefitted from constructive criticism from Dr Mary Ford and two anonymous reviewers.

APPENDIX A: MODEL DESCRIPTION

A1. Equations

The Flamar–Para(o)voz is a '2.5 D' FLAC-like code (Cundall, 1989). It has a mixed finite-difference/finite element numerical scheme, in which the coordinate frame is Cartesian 2D, but stress/strain relations are computed in a 3D formulation. The Lagrangian mesh of Paravoz is composed of quadrilateral elements subdivided onto two couples of triangular sub-elements with tri-linear shape functions. Para(o)voz is a large strain fully explicit time-marching algorithm. It locally solves full Newtonian equations of motion in continuum mechanics approximation:

$$\langle \rho \ddot{\mathbf{u}} \rangle - div\boldsymbol{\sigma} - \rho \mathbf{g} = 0 \qquad \text{(A1)}$$

coupled with constitutive equations:

$$\frac{\mathrm{D}\sigma}{\mathrm{D}t} = F(\sigma,\, \mathbf{u},\, \nabla\dot{\mathbf{u}},\ldots\, T\ldots) \qquad \text{(A2)}$$

and with equations of heat transfer (heat advection $\mathbf{u}\nabla T$ in the equation below is solved separately):

$$\frac{\rho C_\mathrm{p} \mathrm{D}T}{\mathrm{D}t + \dot{\mathbf{u}}\nabla T - k\,\mathrm{div}(\nabla T) - H_\mathrm{r} = 0} \qquad \text{(A3)}$$
$$\rho = \rho_0(1 - \alpha T)$$

Here $\mathbf{u}$, $\boldsymbol{\sigma}$, $\mathbf{g}$ and k are the respective terms for the displacement, stress, acceleration due to body forces and thermal conductivity. The triangular brackets in Eqn. (A1) specify conditional use of the related term [in quasi-static mode inertial terms are dumped using inertial mass scaling (Cundall, 1989)]. The terms t, ρ, C_p, T and H_r designate, respectively, time, density, specific heat, temperature and internal heat production. The terms $\mathrm{D}/\mathrm{D}t$, $\mathrm{D}\sigma/\mathrm{D}t$ and F are a time derivative, an objective (Jaumann) stress time derivative and a functional, respectively. In the Lagrangian method, incremental displacements are added to the grid coordinates allowing the mesh to move and deform with material. This enables solution of large-strain problems locally using a small-strain formulation. On each time step, the solution is obtained in local coordinates, which are then updated in a large-strain mode.

Solution of Eqn. (A1) provides velocities at mesh points used for computation of element strains and of heat advection $\mathbf{u}\nabla T$. These strains are used in Eqn. (A2) to calculate element stresses and equivalent forces as input for the computation of the velocities for the next time step. Owing to the explicit approach, there are no convergence issues, which is rather a common problem of implicit methods in case of nonlinear rheologies. The algorithm automatically checks and adopts the internal time step using 0.1–0.5 of Courant's criterion for propagation of information, which warrants a stable solution.

A2. Explicit EVP rheology

We use a serial (Maxwell type) body [Eqn. (1)], in which total strain increment in each numeric element is defined by a sum of elastic, viscous and brittle strain increments. Consequently, in contrast to fluid dynamic approaches, where nonviscous rheological terms are simulated using pseudo-plastic and pseudo-elastic viscous terms (e.g. Solomatov & Moresi, 2000; Bercovici *et al.*, 2001), our method explicitly treats all rheological terms. The parameters of elastic–ductile–plastic rheology laws for crust and mantle come from rock mechanics data (Tables A1 and A2; Kirby & Kronenberg, 1987; Kohlstedt *et al.*, 1995).

Plastic (brittle) behaviour

The brittle behaviour of rocks is described by Byerlee's law (Byerlee, 1978; Ranalli, 1995), which corresponds to Mohr–Coulomb material with a friction angle $\phi = 30^\circ$ and cohesion $|C_0| < 20$ MPa (e.g. Gerbault *et al.*, 1998):

$$|\tau| = C_0 - \sigma_n \tan\phi \qquad \text{(A4)}$$

where σ_n is normal stress $\sigma_\mathrm{n} = 1/3\sigma_\mathrm{I} + \sigma_\mathrm{II}^\mathrm{dev} \sin\phi$, $1/3\sigma_\mathrm{I} = P$ is the effective pressure and $\sigma_\mathrm{II}^\mathrm{dev}$ is the second invariant of deviatoric stress or effective shear stress. The condition of transition to brittle deformation (function of rupture f) reads as: $f = \sigma_\mathrm{II}^\mathrm{dev} + P\sin\phi - C_0\cos\phi = 0$ and $\partial f/\partial t = 0$. In terms of principal stresses, the equivalent of the yield criterion Eqn. (A5) reads as:

$$\sigma_1 - \sigma_3 = -\sin\phi(\sigma_1 + \sigma_3 - 2C_0/\tan\phi) \qquad \text{(A5)}$$

Elastic behaviour

The elastic behaviour is described by the linear Hooke's law:

$$\sigma_{ij} = \lambda\varepsilon_{ii}\delta_{ij} + 2G\varepsilon_{ij} \qquad \text{(A6)}$$

where λ and G are Lame's constants. Repeating indexes mean summation and δ is Kronecker's operator.

Viscous (ductile) behaviour

Mantle convection and a part of lithospheric deformation is controlled by thermally activated creep (Kirby & Kronenberg, 1987; Ranalli, 1995). Within deep lithosphere and underlying mantle regions, the creeping flow is non-Newtonian as the effective viscosity can vary within 10 orders of magnitude as a function of differential stress:

$$e_{ij}^d = A(\sigma_1 - \sigma_3)^\mathrm{n} \exp(-Q\,R^{-1}T^{-1}) \qquad \text{(A7)}$$

Where $e_{ij}^d = \dot{\varepsilon}_{ij}^d$ is shear strain rate, A is material constant, n is the power law exponent, Q is the activation enthalpy, R is Boltzman's gas constant and T is temperature in degree Kelvins, σ_1 and σ_3 are the principal stresses. The effective viscosity μ_eff for this law is defined as:

$$\tau_{ij} = \mu_\mathrm{eff} e_{ij}^d$$

which yields:

$$\mu_{eff} = e_{ij}^{d(1-n)/n} A^{-1/n} \exp[Q(nRT)^{-1}] \qquad (A8)$$

For non-uniaxial deformation, the law of Eqn. (A8) is converted to a triaxial form, using an invariant of strain rate and geometrical proportionality factors:

$$\mu_{\mathrm{eff}} = e_{ij}^{d(1-n)/n} A^{-1/n} \exp[Q(nRT)^{-1}]$$

where

$$e_{\mathrm{II}}^{d} = [\mathrm{Inv}_{\mathrm{II}}(e_{ij})]^{1/2} \text{ and } A^{*} = 1/2A\,3^{(n+1)/2} \qquad (A9)$$

parameters A, n, Q are experimentally determined material constants (Table A1). Using olivine parameters (Table A1), one can verify that the predicted effective viscosity at the base of the lithosphere is 10^{19}–5×10^{19} Pa s matching post-glacial rebound data (Turcotte & Schubert, 2002). In the depth interval of 200–0 km, the effective viscosity grows from 10^{19} to 10^{25}–10^{27} Pa s with decreasing temperature. Within the adiabatic temperature interval at depth, the dislocation flow law in Eqn. (A8) is replaced by nearly Newtonian diffusion creep, which results in a quasi-constant mantle viscosity of 10^{19}–10^{21} Pa s (e.g. Turcotte & Schubert, 2002). Weinberg & Podladchikov (1994) have also shown that the effective viscosity in close vicinity of an ascending diapir is influenced by the local strain rate field and partly by heat exchanges between the diapir and surrounding rock, which suggests possible changes.

REFERENCES

Alinaghi, A., Koulakov, I. & Thybo, H. (2007) Seismic tomographic imaging of *P*- and *S*-waves velocity perturbations in the upper mantle beneath Iran. *Geophys. J. Int.*, **169**, 1089–1102.

Allen, M.B. & Davies, C.E. (2007) Unstable Asia: active deformation of Siberia revealed by drainage shifts. *Basin Res.*, **19**, 379–392.

Alzaga-Ruiz, H., Granjeon, D., Lopez, M., Seranne, M. & Roure, F. (2008) Gravitational collapse and Neogene sediment transfer across the western margin of the Gulf of Mexico: insights from numerical models. *Tectonophysics*, **470**, 21–41.

Artyushkov, E.V. (2007) Formation of the superdeep Caspian Basin: subsidence driven by phase change in continental crust. *Russ. Geol. Geophys.*, **48**, 1102–1014.

Avouac, J. & Burov, E. (1996) Erosion as a driving mechanism of intracontinental mountain growth. *J. Geophys. Res.*, **101**, 17747–17769.

Axen, G.J., Lam, P.J., Grove, M., Stockli, D.F. & Hassanzadeh, J. (2001) Exhumation of the west-central Alborz Mountains, Iran, Caspian subsidence, and collision-related tectonics. *Geology*, **29**, 559–562.

Bada, G., Horváth, F., Cloetingh, S., Coblentz, D.D. & Tóth, T. (2001) The role of topography induced gravitational stresses in basin inversion: the case study of the Pannonian basin. *Tectonics*, **20**, 343–363.

Bada, G., Horváth, F., Dövényi, P., Szafián, P., Windhoffer, G. & Cloetingh, S. (2007) Present-day stress field and tectonic inversion in the Pannonian basin. *Global Planet. Change*, **58**, 165–180.

Beaumont, C. (1981) Foreland basins. *Geophys. J. R. Astron. Soc.*, **65**, 291–329.

Beaumont, C., Fullsack, P. & Hamilton, J. (1992) Erosional control of active compressional orogens. In: *Thrust Tectonics* (Ed. by K.R. McClay), pp. 1–18. Chapman & Hall, London.

Beekman, F., Bull, J., Cloetingh, S. & Scrutton, R. (1996) Crustal fault reactivation facilitating lithospheric folding/buckling in the Central Indian Ocean. In: *Modern Developments in Structural Interpretation Validation and Modeling* (Ed. by P. Buchanan & D.A. Nieuwland), *Geol. Soc. Lond. Spec. Publ.*, **99**, 251–263.

Beekman, F., Stephenson, R.A. & Korsch, R.J. (1997) Mechanical stability of the Redbank Thrust Zone, Central Australia: dynamic and rheological implications. *Austral. J. Earth Sci.*, **44**, 215–226.

Bercovici, D., Ricard, Y. & Schubert, G. (2001) A two-phase model for compaction and damage 3. Applications to shear localization and plate boundary formation. *J. Geophys. Res.*, **106**, 8925–8939.

Biot, M.A. (1961) Theory of folding of stratified viscoelastic media and its implications in tectonics and orogenesis. *Geol. Soc. Am. Bull.*, **72**, 1595–1620.

Bird, P. (1991) Lateral extrusion of lower crust from under high topography in the isostatic limit. *J. Geophys. Res.*, **96**, 10275–10286.

Bonnet, S., Guillocheau, F., Brun, J-P. & Van den Driessche, J. (2000) Large-scale relief development related to quaternary tectonic uplift of a Proterozoic-Paleozoic basement: the Armorican Massif, NW France. *J. Geophys. Res.*, **105**, 19273–19288.

Bourgeois, O., Ford, M., Diraison, M., Le Carlier de Veslud, C., Gerbault, M., Pik, R., Ruby, N. & Bonnet, S. (2007) Separation of rifting and lithospheric folding signatures in the NW-Alpine foreland. *Int. J. Earth Sci.*, **96**, 1003–1031.

Brunet, M.-F., Korotaev, M.V., Ershov, A.V. & Nikishin, A.M. (2003) The South Caspian basin: a review of its evolution from subsidence modelling. *Sediment. Geol.*, **156**, 119–148.

Bull, J.M. & Scrutton, R.A. (1992) Seismic reflection images of intraplate deformation, central Indian Ocean, and their tectonic significance. *J. Geol. Soc. Lond.*, **149**, 955–966.

Burg, J.P., Davy, P. & Martinod, J. (1994) Shortening of analogue models of the continental lithosphere: new hypothesis for the formation of the Tibetan plateau. *Tectonics*, **13**, 475–483.

Burg, J.P. & Podladchikov, Y. (1999) Lithosphere scale folding: numerical modelling and application to the Himalayan syntaxes. *Int. J. Earth. Sci.*, **88**, 190–200.

Burov, E., Guillou-Frottier, L., d'Acremont, E., le Pourhiet, L. & Cloetingh, S. (2007) Plume head–lithosphere interactions near intra-continental plate boundaries. *Tectonophysics*, **434**, 15–38.

Burov, E.B. & Cloetingh, S. (1997) Erosion and rift dynamics: new thermo-mechanical aspects of post-rift evolution of extensional basins. *Earth Planet. Sci. Lett.*, **150**, 7–26.

Burov, E.B. & Cloetingh, S. (2009) Controls of mantle plumes and lithospheric folding on modes of intra-plate continental tectonics: differences and similarities. *Geophys. J. Int.*, **178**, 1691–1722.

Burov, E.B., Jolivet, L., le Pourhiet, L. & Poliakov, A. (2001) A thermemechanical model of exhumation of HP and UHP methamorphic rocks in Alpine mountain belts. *Tectonophysics*, **342**, 113–136.

Burov, E.B. & Molnar, P. (1998) Gravity anomalies over the Ferghana Valley (Central Asia) and intracontinental deformation. *J. Geophys. Res.*, **103**, 18137–18152.

Burov, E.B., Nikishin, A.M., Cloetingh, S. & Lobkovsky, L.I. (1993) Continental lithosphere folding in central Asia (Part II): constraints from gravity and tectonic modelling. *Tectonophysics*, **226**, 73–87.

Burov, E.B. & Poliakov, A. (2001) Erosion and rheology controls on syn- and post-rift evolution: verifying old and new ideas using a fully coupled numerical model. *J. Geophys. Res.*, **106**, 16461–16481.

Burov, E. & Toussaint, G. (2007) Surface processes and tectonics: forcing of continental subduction and deep processes. *Global Planet. Change*, **58**, 141–164.

Byerlee, J.D. (1978) Friction of rocks. *Pure Appl. Geophys.*, **116**, 615–626.

Calvo, J.P., Daams, R., Morales, J., López Martínez, N., Agustí, J., Anadón, P., Armenteros, I., Cabrera, L., Civis, J., Corrochano, A., Díaz Molina, M., Elizaga, E., Hoios, M., Martín, E., Martínez, J., Moissenet, E., Muñoz, A., Perez García, A., Pérez González, A., Portero, J.M., Robles, F., Santisteban, C., Torres, T., Van der Meulen, A.J., Vera, J.A. & Mein, P. (1993) Up-to-date Spanish continental Neogene synthesis and paleoclimatic interpretation. *Rev. Soc. Geol. España*, **6**, 29–40.

Carter, N.L. & Tsenn, M.C. (1987) Flow properties of continental lithosphere. *Tectonophysics*, **136**, 27–63.

Casas-Sainz, A.M & de Vicente, G. (2009) On the tectonic origin of Iberian topography. *Tectonophysics*, **474**, 214–235.

Chu, D. & Gordon, R.G. (1998) Current plate motions across the Red Sea. *Geophys. J. Int.*, **135**, 313–328.

Cloetingh, S. (1988) Intraplate stresses: a new element in basin analysis. In: *New Perspectives in Basin Analysis* (Ed. by K.L. Kleinspehn & C. Poala), pp. 205–230. Springer-Verlag, New York.

Cloetingh, S., Beekman, F., Van Wees, J.D., Ziegler, P.A. & Sokoutis, D. (2008) Post-rift compressional reactivation potential of passive margins and extensional basins. In: *Compressional Deformation within Passive Margins: Nature, Causes and Effects* (Ed. by H. Johnson, *et al.*) *Geol. Soc. Lond. Spec. Publ.* **306**, 27–70.

Cloetingh, S., Beek van Der, P.A., Rees Van, D., Roep, TH.B., Biermann, C. & Stephenson, R.A. (1992) Flexural interaction and the dynamics of Neogene extensional basin formation in the Alboran-Betic region. *Geo-Mar. Lett.*, **12**, 66–75.

Cloetingh, S., Bada, G., Matenco, L., Lankreijer, A., Horváth, F. & Dinu, C. (2006) Modes of basin (de)formation, lithospheric strength and vertical motions in the Pannonian-Carpathian system: inferences from thermomechanical modelling. *Geological Society, London, Memoirs*, **32**, 207–221.

Cloetingh, S. & Burov, E. (1996) Thermomechanical structure of European continental lithosphere: constraints from rheological profiles and EET estimates. *Geophys. J. Int.*, **124**, 695–723.

Cloetingh, S., Burov, E., Beekman, F., Andeweg, B., Andriessen, P., Garcia-Castellanos, D., de Vicente, G. & Vegas, R. (2002) Lithospheric folding in Iberia. *Tectonics*, **21**, 5, doi: 10.1029/2001TC901031.

Cloetingh, S., Burov, E., Matenco, L., Toussaint, G., Bertotti, G., Andriessen, P.A.M., Wortel, M.J.R. & Spakman, W. (2004) Thermo-mechanical controls on the mode of continental collision in the SE Carpathians (Romania). *Earth Planet. Sci. Lett.*, **218**, 57–76.

Cloetingh, S., Burov, E. & Poliakov, A. (1999) Lithosphere folding: primary response to compression? (from Central Asia to Paris Basin). *Tectonics*, **18**, 1064–1083.

Cloetingh, S. & van Wees, J-D. (2005) Strength reversal in Europe's intraplate lithosphere: transition of basin inversion to lithospheric folding. *Geology*, **33**, 285–288.

Cloetingh, S. & Ziegler, P.A. (2007) Tectonic models for the evolution of sedimentary basins. In: *Treatise on Geophysics*, **Vol. 6** (Ed. by A.B. Watts), pp. 486–611. Elsevier, Amsterdam.

Cloetingh, S., Ziegler, P.A., Beekman, F., Andriessen, P.A.M., Matenco, L., Bada, G., Garcia-Castellanos, D., Hardebol, N., Dèzes, P. & Sokoutis, D. (2005) Lithospheric memory, state of stress and rheology: neotectonic controls on Europe's intraplate continental topography. *Quat. Sci. Rev.*, **24**, 241–304.

Cobbold, P.R., Davy, P., Gapais, E.A., Rossello, E.A., Sadybasakov, E., Thomas, J.C., Tondji Biyo, J.J. & De Urreiztieta, M. (1993) Sedimentary basins and crustal thickening. *Sediment. Geol.*, **86**, 77–89.

Corti, G., Van Wijk, J., Bonini, M., Sokoutis, D., Cloetingh, S., Innocenti, F. & Manneti, P. (2003) Transition from continental break-up to seafloor spreading: how fast, symmetric and magmatic. *Geophys. Res. Lett.*, **30**, 12, doi: 10.1029/2003GL017374.

Cross, T.A. (Ed.) (1989) *Quantitative Dynamic Stratigraphy.* Prentice Hall, Englewood Cliffs, NJ. pp. 127–148.

Cundall, P.A. (1989) Numerical experiments on localization in frictional materials. *Ing. Arch.*, **59**, 148–159.

Decelles, P.G. & Giles, K.A. (1996) Foreland basin systems. *Basin Res.*, **8**, 105–123.

Desegaulx, P., Kooi, H. & Cloetingh, S. (1991) Consequences of foreland basin development on thinned continental lithosphere: application to the Aquitaine basin (SW France). *Earth Planet. Sci. Lett.*, **106**, 116–132.

De Bruijne, C.H. & Andriessen, P.A.M. (2002) Far field effects of Alpine plate tectonism in the Iberian microplate recorded by fault-related denudation in the Spanish Central System. *Tectonophysics*, **349**, 161–184.

De Vicente, G., Cloetingh, S., Muñoz-Martín, A., Olaiz, A., Stich, D., Vegas, R., Galindo-Zaldívar, J. & Fernández-Lozano, J. (2008) Inversion of moment tensor focal mechanisms for active stresses around the Microcontinent Iberia: tectonic implications. *Tectonics*, **27**, TC1009.

De Vicente, G. & Vegas, R. (2009) Large-scale distributed deformation controlled topography along the western Africa–Eurasia limit: tectonic constraints. *Tectonophysics*, **474**, 124–143.

De Vicente, G., Vegas, R., Muñoz Martín, A., Silva, P.G., Andriessen, P., Cloetingh, S., Gonzáles Casado, J.M., Wees van, J-D., Alvarez, J., Carbó, A. & Olaiz, A. (2007) Cenozoic thick-skinned deformation and topography evolution of the Spanish Central System. *Global Planet. Change*, **58**, 335–381.

Devlin, W.J., Cogswellll, J.M., Gaskins, G.M., Isaksen, G.H., Pitcher, D.M., Pius, D.P., Stanley, K.O. & Wall, J.R.T. (1999) South Caspian basin: young, cool, and full of promise. *GSA Today*, **9**, 1–9.

Dèzes, P., Schmid, S.M. & Ziegler, P.A. (2004) Evolution of the European Cenozoic Rift System: interaction of the Alpine and Pyrenean orogens with their foreland lithosphere. *Tectonophysics*, **389**, 1–33.

Dombradi, E., Sokoutis, D., Bada, G., Cloetingh, S. & Horvath, F. (2010) Modelling of recent deformation of the Pannoanian lithosphere: lithospheric folding and tectonic topography. *Tectonophysics*, **484**, 103–118.

Egan, S.S., Mosar, J., Brunet, M.-F. & Kangarli, T. (2009) Subsidence and uplift mechanisms within the South Caspian Basin: insights from the onshore and offshore Azerbaijan region. *Geol. Soc. Lond. Spec. Publ.*, **312**, 219–240.

Elfrink, N.M. (2001) Quaternary groundwater avulsions: evidence for large-scale midcontinent folding? *Assoc. Environ. Eng. Geol. News*, **44**, 60.

Fakhari, M.D., Axen, G.J., Horton, B.K., Hassanzadeh, J. & Amini, A. (2008) Revised age of proximal deposits in the Zagros foreland basin and implications for Cenozoic evolution of the High Zagros. *Tectonophysics*, **451**, 170–185.

Fernandez-Lozano, J., Sokoutis, D., Willingshofer, E., Cloetingh, S., & De Vicente, G. (2010) Cenozoic deformation of Iberia: a model for intraplate mountain building and basin development based on analogue modelling. *Tectonics*, in press.

Garcia-Castellanos, D., Fernandez, M. & Torne, M. (1997) Numerical modelling of foreland basin formation: a program relating thrusting, flexure, sediment geometry and lithosphere rheology. *Comp. Geosci.*, **23**, 993–1003.

Garcia-Castellanos, D., Verges, J., Gaspar-Escribano, J. & Cloetingh, S. (2003) Interplay between the tectonics, climate, and fluvial transport during the Cenozoic evolution of the Ebro Basin (NE Iberia). *J. Geophys. Res.*, **108**, 2347.

Geller, C.A., Weissel, J.K. & Anderson, R.N. (1983) Heat transfer and intraplate deformation in the central Indian Ocean. *J. Geophys. Res.*, **88**, 1018–1032.

Gerbault, M. (2000) At what stress level is the central Indian Ocean lithosphere buckling? *Earth Planet. Sci. Lett.*, **178**, 165–181.

Gerbault, M., Burov, E., Poliakov, A.N.B. & Daignieres, M. (1998) Do faults trigger folding in the lithosphere? *Geophys. Res. Lett.*, **26**, 271–274.

Goetze, C. & Evans, B. (1979) Stress and temperature in the bending lithosphere as constrained by experimental rock mechanics. *Geophys. J. R. Astron. Soc.*, **59**, 463–478.

Gossman, H. (1976) Slope modelling with changing boundary conditions – effects of climate and lithology. *Z. Geomorphol. Suppl.*, **25**, 72–88.

Granjeon, D. (2009) 3D stratigraphic modelling of sedimentary basins, from source to sink. *AAPG Annual Convention and Exhibition*, June 7–10, 2009, Denver, CO.

Grenerczy, Y., Sella, G.F., Stein, S. & Kenyeres, A. (2005) Tectonic implications of the GPS velocity field in the northern Adriatic region. *Geophys. Res. Lett.*, **32**, L16311.

Guest, B., Guest, A. & Axen, G. (2007) Late Tertiary tectonic evolution of northern Iran: a case for simple crustal folding. *Global Planet. Change*, **58**, 435–453.

Guillocheau, F., Robin, C., Allemand, P., Bourqui, S. & Brault, N. (2000) Meso-Cenozoic geodynamic evolution of the Paris Basin: 3D stratigraphic constraints. *Geodin. Acta*, **13**, 189–246.

Guillou-Frottier, L., Burov, E., Nehlig, P. & Wyns, R. (2007) Deciphering plume–lithosphere interactions beneath Europe from topographic signatures. *Global Planet. Change*, **58**, 119–140.

Hafkenscheid, E., Wortel, M.J.R. & Spakman, W. (2006) Subduction history of the Tethyan region derived from seismic tomography and tectonic reconstructions. *J. Geophys. Res.*, **111**, B08401.

Horváth, F. (1995) Phases of compression during the evolution of the Pannonian Basin and its bearing on hydrocarbon exploration. *Mar. Petrol. Geol.*, **12**, 837–844.

Horváth, F., Bada, G., Szafián, P., Tari, G., Ádám, A. & Cloetingh, S. (2006) Formation and deformation of the Pannonian basin: constraints from observational data. *Geol. Soc. Lond. Mem.*, **32**, 191–206.

Horváth, F. & Cloetingh, S. (1996) Stress-induced late-stage subsidence anomalies in the Pannonian basin. *Tectonophysics*, **266**, 287–300.

Huismans, R.S. & Beaumont, C.B. (2002) Asymmetric lithospheric extension: the role of frictional plastic strain softening inferred from numerical experiments. *Geology*, **30**, 211–214.

Hunt, G., Muhlhaus, H., Hobbs, B. & Ord, A. (1996) Localized folding of viscoelastic layers. *Geol. Rundsch.*, **85**, 58–64.

Kaban, M.K. (2002) A gravity model of the north Eurasia crust and upper mantle: 2. The Alpine-Mediterranean fold belt and adjacent structures of the southern former USSR. *Russ. J. Earth. Sci.*, **4**, 19–33.

Kirby, S.H. & Kronenberg, A.K. (1987) Rheology of the lithosphere: selected topics. *Rev. Geophys.*, **25**, 1219–1244.

Kirkby, M.J. (1986) A two-dimensional model for slope and stream evolution. In: *Hillslope Processes* (Ed. by A.D. Abrahams), pp. 203–224. Allen and Unwin, Boston.

Kohlstedt, D.L., Evans, B. & Mackwell, S.J. (1995) Strength of the lithosphere: constraints imposed by laboratory experiments. *J. Geophys. Res.*, **100**, 17587–17602.

Kombrink, H., Leever, K.A., Van Wees, J-D., Van Bergen, F., David, P. & Wong, T.E. (2008) Late Carboniferous foreland basin formation and Early Carboniferous stretching in Northwestern Europe: inferences from quantitative subsidence analyses in the Netherlands. *Basin Res.*, **20**, 377–395.

Kooi, H. & Beaumont, C. (1994) Escarpment evolution on high-elevation rifted margins: insights derived from a surface processes model that combines diffusion, advection and reaction. *J. Geophys. Res.*, **99**, 12191–12210.

Lagarde, J.L., Baize, S., Amorese, D., Delccaillau, B., Fort, M. & Volant, V. (2000) Active tectonics, seismicity and geomorphology with special reference to Normandy (France). *J. Quat. Sci.*, **15**, 745–758.

Lambeck, K. (1983) The role of compressive forces in intracratonic basin formation and mid-plate orogenies. *Geophys. Res. Lett.*, **10**, 845–848.

Lavier, L.L. & Steckler, M.S. (1997) The effect of sedimentary cover on the flexural strength of the continental lithosphere. *Nature*, **389**, 476–479.

Lawrence, D.T., Doyle, M. & Aigner, T. (1990) Stratigraphic simulation of sedimentary basins: concepts and calibration. *AAPG Bull.*, **74**, 273–295.

Leeder, M.R. (1991) Denudation, vertical crustal movements and sedimentary basin infill. *Geol. Rundsch.*, **80**, 441–458.

Lefort, J-P. & Agarwal, B.N. (1996) Gravity evidence for an Alpine buckling of the crust beneath the Paris Basin. *Tectonophysics*, **258**, 1–14.

Lefort, J.P. & Agarwal, B.N. (2000) Gravity and geomorphological evidence for a large crustal bulge cutting across Brittany (France): a tectonic response to the closure of the Bay of Biscay. *Tectonophysics*, **323**, 149–162.

Lefort, J.P. & Agarwal, B.N. (2002) Topography of the Moho undulations in France from gravity data: their age and origin. *Tectonophysics*, **350**, 193–213.

Leighton, M.W. & Kolata, D.R. (1990) Selected interior cratonic basins and their place in the scheme of global tectonics: a synthesis. In: *Interior Cratonic Basins* (Ed. by M.W. Leighton, D.R. Kolata, D.F. Oltz & J.J. Eidel). *AAPG Memoir*, **51**, 729–797.

Lenotre, N., Thierry, P., Blanchin, R. & Brochard, G. (1999) Current vertical movement demonstrated by comparative levelling in Brittany (France). *Tectonophysics*, **301**, 333–344.

Le Solleuz, A., Doin, M.-P., Robin, C. & Guillocheau, F. (2004) From a mountain belt collapse to a sedimentary basin development: 2-D thermal model based on inversion of stratigraphic data in the Paris Basin. *Tectonophysics*, **386**, 1–27.

Li, S., Mooney, W.D. & Fan, J. (2006) Crustal structure of mainland China from deep seismic sounding data. *Tectonophysics*, **420**, 239–252.

Littke, R., Bayer, U., Gajewski, D. & Nelskamp, S. (2008) *Dynamics of Complex Intracontinental Basins*. Springer, Berlin.

Liu, M., Mooney, W.D., Li, S., Okaya, N. & Detweiler, S. (2006) Crustal structure of the northeast margin of the Tibetan plateau from the Songpan-Ganzi terrane to the Ordos basin. *Tectonophysics*, **420**, 253–266.

Liu, Y., Neubauer, F., Genser, J., Ge, X., Takasu, A., Yuan, S., Chang, L. & Li, W. (2007) Geochronology of the initiation and displacement of the Altyn strike-slip fault, western China. *J. Asian Earth Sci.*, **29**, 243–252.

Lundin, E.R. & Doré, A.G. (1997) A tectonic model for the Norwegian passive margin with implications for the NE Atlantic: early Cretaceous to break-up. *J. Geol. Soc.*, **154**, 545–550.

Marotta, A.M., Bayer, U. & Thybo, H. (2000) The legacy of the NE German Basin – reactivation by compressional buckling. *Terra Nova*, **12**, 132–14.

Martinod, J. & Davy, P. (1992) Periodic instabilities during compression or extension of the lithosphere: 1. Deformation modes from an analytical perturbation method. *J. Geophys. Res.*, **97**, 1999–2014.

Martinod, J. & Davy, P. (1994) Periodic instabilities during compression of the lithosphere: 2. Analogue experiments. *J. Geophys. Res.*, **99**, 12057–12069.

Matenco, L., Bertotti, G., Leever, K., Cloetingh, S., Schmid, S., Tărăpoancă, M. & Dinu, C. 2007 Large-scale deformation in a locked collisional boundary: interplay between subsidence and uplift, intraplate stress, and inherited lithospheric structure in the late stage of the SE Carpathians evolution. *Tectonics*, **26**, TC4011.

Mazur, S., Scheck-Wenderoth, M. & Krzywiec, P. (2005) Different modes of the Late Cretaceous – early tertiary inversion in the North German and Polish basins. *Int. J. Earth Sci.*, **94**, 782–798.

McAdoo, D.C. & Sandwell, D.T. (1985) Folding of the oceanic lithosphere. *J. Geophys. Res.*, **90**, 8563–8569.

Mckenzie, D.P. (1978) Some remarks on the development of sedimentary basins. *Earth Planet. Sci. Lett.*, **95**, 53–72.

Muehlhaus, H.B., Sahaguchi, H. & Hobbs, B.E. (1998) Evolution of three-dimensional folds for a non Newtonian plate in a viscous medium. *Proc. R. Soc. London, Ser A, Math. Phys. NG. Sci.*, **454**, 3121–3143.

Nadirov, R.S., Bagirov, E., Tagiyev, M. & Lerche, I. (1997) Flexural plate subsidence, sedimentation rates and structural development of the super-deep south Caspian Basin. *Mar. Petrol. Geol.*, **14**, 383–400.

Naylor, M. & Sinclair, H.D. (2007) Punctuated thrust deformation in the context of doubly vergent thrust wedges: implications for the localization of uplift and exhumation. *Geology*, **35**, 559–562.

Naylor, M. & Sinclair, H.D. (2008) Pro- vs. retro foreland basins. *Basin Res.*, **20**, 1365–2117.

Necea, D., Fielitz, W. & Matenco, L. (2005) Late Pliocene-quaternary tectonics in the frontal part of the SE Carpathians: insights from tectonic geomorphology. *Tectonophysics*, **410**, 137–156.

Nikishin, A.M., Brunet, M.F., Cloetingh, S. & Ershov, A.V. (1997) Northern Peri-Tethyan Cenozoic intraplate deformations: influence of the Tethyan collision belt on the Eurasian continent from Paris to Tian-Shan. *C. R. Acad. Sci., Ser. IIa: Sci. Terre Planets*, **234**, 49–57.

Nikishin, A.M., Cloetingh, S., Lobkovsky, L. & Burov, E.B. (1993) Continental lithosphere folding in Central Asia (Part I): constraints from geological observations. *Tectonophysics*, **226**, 59–72.

Nikishin, A.M., Korotaev, M.V., Ershov, A.V. & Brunet, M.F. (2003) The Black Sea Basin: tectonic history and Neogene-Quaternary rapid subsidence modelling. *Sediment. Geol.*, **156**, 149–168.

Perez-Gussinye, M. & Watts, A.B. (2005) The long-term strength of Europe and its implications for plate-forming processes. *Nature*, **436**, 381–384.

Pitman, W.C. & Golovchenko, X. (1983) The effect of sea-level change on the shelf edge and slope of passive margin. In: *The Shelf Break: Critical Interface on Continental Margins* (Ed. by D.J. Stanlay & G.T. Moore), *SEPM Spec. Publ.*, **33**, 41–58.

Quinlan, G. (1987) Models of subsidence mechanisms in intracratonic basins and their applicability to North American examples. *Can. Soc. Pet. Geol. Mem.*, **12**, 463–481.

Quinlan, G. & Beaumont, C. (1984) Appalachian thrusting, lithospheric flexure and the Paleozoic stratigraphy of the eastern interior of North America. *Can. J. Earth Sci.*, **21**, 973–996.

Ramberg, H. (1961) Contact strain and folding instability of multilayered body under compression. *Geol. Rundsch.*, **51**, 405–439.

Ranalli, G. (1995) *Rheology of the Earth*, 2nd edn. Chapman & Hall, London.

Ritter, J.R.R., Jordan, M., Christensen, U.R. & Achauer, U. (2001) A mantle plume under the Eifel volcanics fields, Germany. *Earth Planet. Sci. Lett.*, **186**, 7–14.

Ritzmann, O. & Faleide, J.I. (2009) The crust and mantle lithosphere in the Barents Sea/Kara Sea region. *Tectonophysics*, **470**, 89–104.

Robin, C., Allemand, P., Burov, E., Doin, M.P., Guillocheau, F., Dromart, G. & Garcia, J.P. (2003) Vertical movements of the Paris Basin (Triassic–Pleistocene): from 3D stratigraphic database to numerical models. In: *New Insights in Structural Interpretation and Modelling* (Ed. by P. Buchanan & D.A. Nieuwland), *Geol. Soc. London Spec. Publ.*, **212**, 225–250.

Roure, F., Cloetingh, S., Scheck-Wenderoth, M. & Ziegler, P.A. (2010) Achievements and challenges in sedimentary basin dynamics: a review. In: *New Frontiers in Integrated Solid Earth Sciences* (Ed. by S. Cloetingh & J. Negendank), pp. 145–233. Springer-Verlag, Berlin.

Royden, L. (1988) Flexural behaviour of the continental lithosphere in Italy: constraints imposed by gravity and deflection data. *J. Geophys. Res.*, **93**, 7747–7766.

Royden, L.H. (1993) The tectonic expression of the slab pull at continental convergent boundaries. *Tectonics*, **12**, 303–325.

Sacchi, M., Horvath, F. & Magyari, O. (1999) Role of unconformity bounded units in the stratigraphy of the continental record: a casestudy from the Late Miocene of the western Pannonian basin, Hungary. *Geol. Soc. London Spec. Publ.*, **156**, 357–390.

Scheck, M. & Bayer, U. (1999) Evolution of the Northeast German Basin – inferences of a 3D structural model and subsidence analysis. *Tectonophysics*, **373**, 55–73.

SCHMALHOLTZ, S.M. & PODLADCHIKOV, Y.Y. (2000) Finite amplitude folding: transition from exponential to taper length controlled growth. *Earth Planet. Sci. Lett.*, **181**, 619–633.

SCHUBERT, G., TURCOTTE, D.L. & OLSON, P. (2001) *Mantle Convection in the Earth and Planets*. Cambridge University Press, Cambridge, UK.

SHIN, Y.H., SHUM, C.-K., BRAITENBERG, C., LEE, S.M., XU, H., CHOI, K.S., BAEK, J.H. & PARK, J.U. (2009) Three-dimensional fold structure of the Tibetan Moho from GRACE gravity data. *Geophys. Res. Lett.*, **36**, L01302.

SMIT, J., BRUN, J.P., CLOETINGH, S. & BEN-AVRAHAM, Z. (2008) Pull-apart basin formation and development in narrow transform zones with application to the Dead Sea Basin. *Tectonics*, **27**, TC6018.

SMIT, J., BRUN, J.P., CLOETINGH, S. & BEN-AVRAHAM, Z. (2010) The rift-like structure and asymmetry of the Dead Sea Fault. *Earth Planet. Sci. Lett.*, **290**, 74–82.

SMITH, R.B. (1979) The folding of a strongly non-Newtonian layer. *Am. J. Sci.*, **79**, 272–287.

SOKOUTIS, D., BURG, J.P., BONINI, M., CORTI, G. & CLOETINGH, S. (2005) Lithospheric-scale structures from the perspective of analogue continental collision. *Tectonophysics*, **406**, 1–15.

SOLOMATOV, V.S. & MORESI, L.N. (2000) Scaling of time-dependent stagnant lid convection; application to small-scale convection on Earth and other terrestrial planets. *J. Geophys. Res.*, **105**, 21795–21817.

STEIN, C.A., CLOETINGH, S. & WORTEL, R. (1989) Seasat-derived gravity constraints on stress and deformation in the northeastern Indian Ocean. *Geophys. Res. Lett.*, **16**, 823–826.

STEL, H., CLOETINGH, S., HEEREMANS, M. & VAN DER BEEK, P.A. (1993) The kinematics of anorogenic basement tectonics and the origin of sedimentary basins. *Tectonophysics*, **226**, 285–299.

STEPHENSON, R. & LAMBECK, K. (1985) Isostatic response of the lithosphere with in-plane stress: application to Central Australia. *J. Geophys. Res.*, **90**, 8581–8588.

STEPHENSON, R.S. & CLOETINGH, S. (1991) Some examples and mechanical aspects of continental lithospheric folding. *Tectonophysics*, **188**, 27–37.

STEPHENSON, R.S., RICKETTS, B.D., CLOETINGH, S. & BEEKMAN, F. (1990) Lithosphere folds in the Eurekan orogen, Arctic Canada? *Geology*, **18**, 603–606.

TARAPOANCA, M., BERTOTTI, G., MATENCO, L., DINU, C. & CLOETINGH, S. (2003) Architecture of the Focsani depression: a 13 km deep basin in the Carpathians bend zone (Romania). *Tectonics*, **22**, 1074.

TER VOORDE, M., DE BRUIJNE, C.H., CLOETINGH, S.A.P.L. & ANDRIESSEN, P.A.M. (2004) Thermal consequences of thrust faulting: simultaneous versus successive fault activation and exhumation. *Earth Planet. Sci. Lett.*, **223**, 395–413.

TESAURO, M., HOLLENSTEIN, C., EGLI, R., GEIGER, A. & KAHLE, H.-G. (2005) Continuous GPS and broad-scale deformation across the Rhine Graben and the Alps. *Int. J. Earth. Sci.*, **94**, 525–537.

TESAURO, M., KABAN, M., CLOETINGH, S., HARDEBOL, N. & BEEKMAN, F. (2007) 3D strength and gravity anomalies of the European lithosphere. *Earth Planet. Sci. Lett.*, **263**, 56–73.

THOMAS, J.C., COBBOLD, P.R., SHEIN, V.S. & LE DOUARAN, S. (1999a) Sedimentary record of late Paleozoic to recent tectonism in central Asia - analysis of subsurface data from the Turan and south Kazak domains. *Tectonophysics*, **313**, 243–263.

THOMAS, J.C., GRASSO, J.R., BOSSU, R., MARTINOD, J. & NURTAEV, B. (1999b) Recent deformation in the Turan and South Kazakh platforms, western central Asia, and its relation to Arabia–Asia and India–Asia collisions. *Tectonics*, **18**, 201–214.

TIKOFF, B. & MAXSON, J. (2001) Lithospheric buckling of the Laramide foreland during Late Cretaceous and Paleogene, western United States. *Rocky Mt. Geol.*, **36**, 13–35.

TURCOTTE, D.L. & SCHUBERT, G. (2002) *Geodynamics, Applications of Continuum Physics to Geological Problems*, 2nd edn. Cambridge University Press, Cambridge, UK.

VAN BALEN, R.T., VAN DER BEEK, P.A. & CLOETINGH, S. (1995) The effect of rift shoulder erosion on stratal patterns at passive margins: implications for sequence stratigraphy. *Earth Planet. Sci. Lett.*, **134**, 527–544.

VAN DER BEEK, P., ANDRIESSEN, P.A.M. & CLOETINGH, S. (1995) Morphotectonic evolution of rifted continental margins: inferences from a coupled tectonic-surface processes model and fission track thermochronology. *Tectonics*, **14**, 406–421.

VAN DER PLUIJM, B., CRADDOCK, J.P., GRAHAM, B.R. & HARRIS, J.H. (1997) Paleostress in cratonic North America: implications for deformation of continental interiors. *Science*, **277**, 794–796.

VAN WEES, J-D. & CLOETINGH, S. (1996) 3D flexure and intraplate compression in the North Sea basin. *Tectonophysics*, **266**, 343–359.

VAN WEES, J.D., VAN BERGEN, F., DAVID, P., NEPVEU, M., BEEKMAN, F. & CLOETINGH, S. (2009) Probabilistic Tectonic heat flow modelling for basin maturation: method and applications. *Mar. Petrol. Geol.*, **26**, 536–551.

VERGES, J. (1999) Estudi Geologic Del Vessant Sud Del Pirineu Oriental I Central. Evolució cinemàtica en 3D. *Collecció Monografies tècniques*, 7, Institut Cartogràfic de Catalunya, Barcelona, 194 pp.

VERMEESCH, P., POORT, J., DUCHKOV, A.D., KLERKX, J. & DE BATIST, M. (2004) Lake Issyk-Kul (Tien Shan): unusually low heat flow in an active intramountane basin. *Russ. Geol. Geophys.*, **45**, 616–625.

VERNANT, P., NILFOROUSHAN, F., HATZFELD, D., ABBASSI, M.R., VIGNY, C., MASSON, F., NANKALI, H., MARTINOD, J., ASHTIANI, A., BAYER, R., TAVAKOLI, F. & CHERY, J. (2004) Present-day crustal deformation and plate kinematics in the Middle East constrained by GPS measurements in Iran and northern Oman. *Geophys. J. Int.*, **157**, 381–398.

WATTS, A.B. & BUROV, E.B. (2003) Lithospheric strength and its relationship to the elastic and seismogenic layer thickness. *Earth. Planet. Sci. Lett.*, **213**, 113–131.

WEINBERG, R.F. & PODLADCHIKOV, Y. (1994) Diapiric ascent of magmas through power law crust and mantle. *J. Geophys. Res.*, **99**, 9543–9559.

WILGUS, C.K., HASTINGS, B.S., KENDALL, C.G.ST.C., PASAMENTIER, H.W., ROSS, C.A. & VAN WAGONER, J.C. (1988) Sea-level changes – an integrated approach. *Spec. Pub. Soc. Econ. Pal. Min.*, **42**, 402 pp.

WORTEL, M.J.R. & SPAKMAN, W. (2000) Subduction and slab detachment in the Mediterranean Carpathian region. *Science*, **290**, 1910–1917.

XIE, X. & HELLER, P.L. (2009) Plate tectonics and basin subsidence history. *Geol. Soc. Am. Bull.*, **121**, 55–64.

ZHAO, J., MOONEY, W.D, ZHANG, X., LI, Z., JIN, Z. & OKAYA, N. (2006) Crustal structure across the Atltyn Tagh Range at the northern margin of the Tibetan plateau and tectonic implications. *Earth Planet. Sci. Lett.*, **241**, 804–841.

Ziegler, P.A., Cloetingh, S. & van Wees, J-D. (1995) Dynamics of intraplate compressional deformation: the Alpine foreland and other examples. *Tectonophysics*, **252**, 7–59.

Ziegler, P.A. & Dèzes, P. (2006) Crustal evolution of Western and Central Europe. In: *European Lithosphere Dynamics* (Ed. by D.G. Gee & R.A. Stephenson), *Geol. Soc. Lond. Mem.*, **32**, 43–56.

Ziegler, P.A. & Dèzes, P. (2007) Cenozoic uplift of Variscan Massifs in the Alpine foreland: timing and controlling mechanisms. *Global Planet. Change*, **58**, 237–269.

Ziegler, P.A., Van Wees, J-D. & Cloetingh, S. (1998) Mechanical controls on collision-related compressional intraplate deformation. *Tectonophysics*, **300**, 103–129.

Zoetemeijer, R., Cloetingh, S., Sassi, W. & Roure, F. (1993) Modelling of piggy-back basin stratigraphy: record of tectonic evolution. *Tectonophysics*, **226**, 253–269.

Zoetemeijer, R., Tomek, C. & Cloetingh, S. (1999) Flexural expression of European continental lithosphere under the western outer Carpathians. *Tectonics*, **18**, 843–861.

Manuscript received 17 August 2009; Manuscript accepted 3 June 2010.

